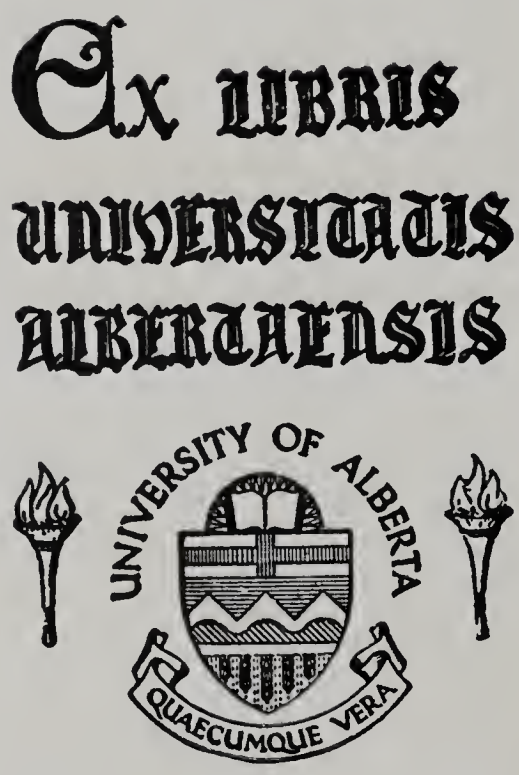

University of Alberta
Printing Department

THE UNIVERSITY OF ALBERTA

THE STUDY OF THE 3.62 MEV. STATE IN Si^{29} VIA THE REACTION $Mg^{26}(\alpha,n\gamma)Si^{29}$

by

James Gordon McLarnon

A THESIS

SUBMITTED TO THE FACULTY OF GRADUATE STUDIES

IN PARTIAL FULFILMENT OF THE REQUIREMENTS FOR THE DEGREE

OF MASTER OF SCIENCE

DEPARTMENT OF PHYSICS

EDMONTON, ALBERTA

October, 1965

THE UNIVERSITY OF ALBERTA

FACULTY OF GRADUATE STUDIES

The undersigned certify that they have read and recommend to the Faculty of Graduate Studies for acceptance a thesis entitled, The Study of the 3.62 MeV State in Si^{29}," submitted by JAMES GORDON McLARNON in partial fulfilment of the requirements for the degree of Master of Science.

ABSTRACT

The $Mg^{26}(\alpha,n\gamma)Si^{29}$ reaction has been used to study the low-lying states of Si^{29}, in particular the first odd parity level which occurs at 3.62 Mev. The 3.62 Mev state had previously been ascertained to have a spin of $^5/_2$ or $^7/_2$ from the characteristic ℓ=3 stripping curve for the protons from the reaction $Si^{28}(d,p)Si^{29}$. The present experiment concludes that the spin is $^7/_2$.

The results of the experiment are interpreted in lieu of the predictions of the nuclear model which is found to be most applicable to Si^{29}, the Nilsson generalized single particle model. A spin assignment of $^7/_2$ to the 3.62 Mev state implies an oblate shape for Si^{29} and also for the rotational core, Si^{28}. It has previously been found that Al^{28} possesses a prolate shape, hence the nuclear deformation changes sign in the mass region at A=28.

ACKNOWLEDGMENTS

Firstly, for his patient work in checking over the thesis before submission and also for his help during the course of the experiment, I thank my supervisor Dr. W. C. Olsen

I am also indebted to Dr. H. W. Taylor and Dr. J. T. Sample for their helpful suggestions pertaining to the experiment.

The help received from the technical staff, in particular Mr. Lars Holm and Mr. Jock Elliott is greatly appreciated.

Thanks are also due to Dr. W. K. Dawson, W. G. Davies, and T. B. Grandy who wrote the computer programs used in the analysis.

Finally the help of Miss Greta Tratt who typed the formula section is to be acknowledged. Thanks also to Emma.

Table of Contents

ILLUSTRATIONS

CHAPTER I

1.1 The Experimental Problem and Procedure

In general, the principal objective of low energy nuclear spectroscopy is to gather significant information relating to the physical properties of nuclei. Once sufficient data regarding some properties have been accumulated, the theoretical predictions of the various models originated to describe these physical properties must be compared with the experimental data, resulting in either a confirmation or rejection of a particular model to describe a given nucleus. It may be possible in the future that a complete mathematical description of the physical properties of all nuclei will be encompassed in some unified model but at present several distinct models are required to explain the spectroscopic features of the low-lying states in nuclei.

The essence of the present experiment is to examine, by means of angular distribution and correlation techniques, the nucleus Si^{29}, and in particular to measure the spin of the first odd parity state which occurs at 3.62 Mev. The results of the experiment will then be compared with the predictions of the model found to be particularily applicable to the mass region A=25 (Li 58), the rotational collective model, or as is sometimes referred to when the nucleus consists of an extra nucleon outside an even-even core, the Nilsson generalized single particle model. Previous experimental evidence will be presented which confirms the relevance of the rotational model to the A=29 system and which does not support the application of two other models which might be expected to have some significance in describing

the Si^{29} nucleus. They are:

(1) The extreme single particle model which has been found to be especially amenable in describing the properties of nuclei near the magic numbers.

(2) The vibrational model which exhibits collective effects similar to the rotational model.

A further elaboration of these models will be given in 1.3.

The reaction employed to study the 3.62 Mev. level of Si^{29} was $Mg^{26}(\alpha,n\gamma)Si^{29}$ and the analysis was carried out using the angular distribution formulas given in method 2 (Li 60) and which are developed in 1.2. In this reaction a compound state in Si^{30} is formed which subsequently decays, via neutron emission, to the residual states of Si^{29}.

A triple correlation is specified by first defining the beam direction as a reference axis and then measuring the correlation of the gamma ray, in coincidence with neutrons, with respect to this axis. Since the orbital angular momentum of the neutrons is perpendicular to their direction of motion, the orbital magnetic quantum number is zero for neutrons detected along the axis defined by the beam direction. The magnetic substates of the residual states in Si^{29} which are then populated will not exceed the vector sum of the remaining angular momenta involved in the reaction, that is the intrinsic spins of the incident particle and neutron, and the ground state spin of the target nucleus. In this particular reaction, in which an even-even nucleus is bombarded with the spinless alpha particle, and assuming a point neutron detector located on the beam axis, only the $m=\pm^1/_2$ magnetic

substates of the residual state will be populated. If the spin of the residual state is greater than $^1/_2$, one can then expect an anisotropic distribution of gamma radiation about the beam axis because the residual state has unequally populated magnetic substates and hence is effectively aligned. Under actual experimental conditions, the neutron detector which is located on the beam axis, subtends a finite solid angle from the source and the population of higher substates may be effected. The probability of occupation however, decreases as the magnetic quantum number increases.

The 3.62 Mev state in Si^{29} decays to a lower state of spin and parity $^5/_2^+$ at 2.03 Mev. by the emission of a 1.59 Mev. gamma ray. Holt and Marsham (Ho 53) have studied the 3.62 Mev. state with the stripping reaction $Si^{28}(d,p)Si^{29}$. They found a characteristic stripping curve for the protons corresponding to $\ell=3$, which restricts the spin assignment to the 3.62 Mev. level to either $^5/_2$ or $^7/_2$ with odd parity.

A theoretical analysis carried out prior to the experiment revealed an important consideration, namely that theoretical curves for the angular distribution of the 1.59 radiation could be drawn for the two possible spin assignments. In general this would not be possible since in addition to the population parameters being unknown, there is an additional undetermined quantity, the mixing ratio δ (the square of which gives the ratio of quadrupole to dipole intensity). In general, the probability of emission of multipole radiation diminishes rapidly as the multipole order increases. For the case of an E1-M2 mixture, as would occur for the 1.59 radiation, and the non-violation of such selection rules as isotopic spin

and K-selection, which might inhibit the E1 component of radiation, the mixing ratio would be very small. The E1 transition from the first odd parity state in Ne^{20}, at 4.97 Mev, has been found to be suppressed by both selection rules (No 63), however the mixing ratio is still found to be small, 0.08 (C1 61).

The two theoretical correlation functions, corresponding to the two possible spins for the 3.62 Mev. state, were found to differ markedly. For a $^5/_2^- \rightarrow {}^5/_2^+$ transition, the correlation intensity reached a maximum at 0° and a minimum at 90° with a ratio of almost two between the two intensities. On the other hand, a $^7/_2^- \rightarrow {}^5/_2^+$ transition indicates an intensity maximum at 90° and a minimum at 0° with a similar intensity ratio between the two. It was also ascertained that even allowing for a substantial mixing ratio ($|\delta|<0.4$) and the population of the $m=\pm {}^3/_2$ magnetic substates, the predicted correlation for a $^5/_2$ spin assignment to the 3.62 Mev. state retains a strong maximum at 0°.

The comparison of the experimental results with the predicted correlation is thus straight-forward and an unambiguous spin assignment to the 3.62 Mev. level is possible. Before discussing the experimental procedure and results, the development of the angular distribution formulas, from which the theoretical predictions are derived, is given in 1.2. Also, previous experimental data regarding the physical properties of nuclei in the mass region A=29 are presented and discussed from nuclear model applications, so that the results of the present experiment can be compared with model predictions.

1.2 Angular Distribution Theory

Two types of formalism can be utilized to describe the angular distribution of radiation from an aligned or polarized nucleus.

1. The use of the density matrix is particularly convenient when the behavior of statistical ensembles is to be considered. This method is especially suitable to the study of polarized radiation.

2. An alternative approach is to expand some Hamiltonian, which describes the interaction between the radiation and the nucleus, in terms of rotation matrices and angular momentum coupling coefficients. The square of the matrix element of the Hamiltonian taken between the initial and final states will give the probability of a transition between the states.

It is the latter formalism which will be subsequently developed.

Assuming that an aligned nucleus has been formed in a nuclear reaction as a result of unequally populating the magnetic substates of a given state, then the total angular distribution of gamma radiation from this state is given by the product of the distribution from the m^{th} magnetic substate $W_m(\theta)$ and the population of that substate $P(m_i)$, summed over all possible magnetic substates.

$$W(\theta) = \sum_{m_i} P(m_i)\, W_m(\theta)$$

Considering the probability of emission of radiation at an angle θ,

specified with respect to some axis usually defined by the incident beam, one can write an analogous equation to the above. Denoting the probability of emission by $W(\theta,c)$, where c is the polarization of the radiation, then

$$W(\theta c) = \sum_{\substack{m_i \\ m_f}} P(m_i) \left| \langle j_i m_i \mid H \mid j_f\ m_f \rangle \right|^2 \qquad (1)$$

The squared matrix element gives the probability of a transition from some initial state $\langle j_i\ m_i \mid$ to a final state $\mid j_f\ m_f\rangle$. The Hamiltonian describing the interaction between the emitted radiation and the nucleus can be written in the form:

$$H = \sum_{LM} \alpha_{LM}\ (c)\ T^L_M \qquad (2)$$

Here the $\alpha_{LM}(c)$ are functions of the polarization of the emitted radiation only, and the T^L_M represents the components of a tensor operator of degree L operating on the wave function describing the nucleus. It should be noted that for no mixing of different multipolarities of radiation, no summation over L is required. If we now consider a rotation of the coordinate system through the Euler angles α, β, and γ, the tensor operator will transform by

$$T^L_M = \sum_{\mu} T^{\mu}_L\ D^L_{\mu M}\ (\alpha,\beta,\gamma) \qquad (3)$$

where $D^{L}_{\mu M}(\alpha,\beta,\gamma)$ is the rotational matrix. In the particular case when the radiation is emitted at some angle θ with respect to a quantization axis, the rotational matrix becomes $D^{L}_{\mu M}(0,\theta,0)$.

Substituting equation (3) into (2) gives

$$H = \sum_{LM} \alpha_{LM}(c) \; T^{\mu}_{L} \; D^{L}_{\mu M}(0,\theta,0) \qquad (4)$$

Putting the Hamiltonian of (4) into the matrix elements of (1), and utilizing the fact that the nuclear states are dependent only on the tensor operator T^{μ}_{L}, one has

$$W(\theta c) = \sum_{m_i} \sum_{LM\mu} P(m_i) \alpha_{LM'}(c) \; \overline{\alpha}_{LM}(c) \; D^{L}_{\mu' M'}(0,\theta,0) \; \overline{D}^{L}_{\mu M}(0,\theta,0)$$
$$m_f \quad M'\mu'$$

$$\times \; \langle j_f m_f \mid T^{\mu'}_{L} \mid j_i m_i \rangle \langle \overline{j_f m_f \mid T^{\mu}_{L} \mid j_i m_i} \rangle \qquad (5)$$

To simplify this expression it is necessary to consider the product of two rotation matrices; this product is termed the Clebsch-Gordon series and it can be written in the following form.

$$\overline{D}^{L}_{\mu M} \; D^{L}_{\mu' M'} = \sum_{k,m',m} (LL\mu\mu' \mid km) \; D^{k}_{m'm} \; (LLM\,M' \mid km') \qquad (5')$$

Also, the two matrix elements appearing in (5) can be related to the

product of a Clebsch-Gordon coefficient and an M independent, reduced matrix element with the use of the Wigner-Eckhart theorem. Denoting a general matrix element by $(\tau'J'M' \mid T^{\mu}_{L} \mid \tau JM)$ where the τ represents any quantum numbers other than J or M, the theorem states

$$(\tau'J'M' \mid T^{\mu}_{L} \mid \tau JM) = (2J + 1)^{-1/2} (JLM\mu \mid J'M') (\tau'J' \mid\mid T^{\mu}_{L} \mid\mid \tau J) \qquad (5'')$$

The reduced matrix element, which contains no M dependence and hence is independent of the geometry involved, will not affect the angular distribution of the emitted radiation and thus can be dropped from further considerations. Substituting the right hand sides of 5' and 5'' into equation 5 yields the following expression for the angular distribution of the polarized radiation.

$$W(\theta c) = \sum_{\substack{m_i \\ m_f}} \sum_{\substack{MM' \\ \mu\mu'}} \sum_{\substack{k \\ m \\ m'}} P(m_i) \propto_{LM} (c) \; \bar{\alpha}_{LM} (c) \; D^{k}_{mm'}(0,\theta,0)$$

$$\times \; (LL\mu\mu' \mid km)(LLMM' \mid km') \; (j_i L \; m_i - \mu' \mid j_f \; m_f)$$

$$\times \; (j_i L \; m_i - \mu \mid j_f \; m_f) \qquad (6)$$

The summation over some of the magnetic quantum numbers is carried out in the appendix and the distribution function takes the simplified form

$$W(\theta,c) = \sum_{k,m} (-1)^{k+j_i-m_i} C_{km}(LL) \; W(j_f \; j_i \; Lk, \; L \; j_i) \; P(m_i)$$

$$\times \; (j_i \; j_i \; m_i - m_i \mid k_0) \; D_{0m}(0,\theta,0) \qquad (7)$$

The Racah coefficient $W(j_f j_i\ Lk;\ L\ j_i)$ represents the coupling of three angular momenta; the spins of the initial and final states of the nucleus, denoted by j_i and j_f respectively, and the angular momentum of the emitted radiation. Specifically, the Racah coefficient is given by

$$W(j_f\ j_i\ L\ k;\ L\ j_i) = \sum_{\substack{m_i \\ m_f}} (-1)^{2j_i+j_f+m+m_i} (2j_i+1)^{-1/2}$$

$$\times\ (2L+1)^{-1/2} (j_f\ j_i\ m_f\ m_i | Lm)(j_i j_i\ m_i m_i \mid km)$$

$$\times\ (j_f L\ m_f\ m \mid j_i m_i)\ (LL\ mm \mid km) \qquad (8)$$

The $C_{km}(LL)$ is termed the radiation parameter and is given by

$$C_{km}(LL) = \sum_{M,M'} (-1)^{L-M}\ \overline{\alpha}_{LM}(c)\ \alpha_{LM'}(c)\ (LLM'-M \mid km) \qquad (9)$$

This parameter depends upon the type of radiation emitted and if no mixing occurs for the radiative transition, the Clebsch-Gordon coefficient has the property

$$(LLM'-M \mid km) \equiv 0 \qquad \text{unless } m = 0$$

Thus the radiation parameter can be written as $C_{k0}(LL)$ where

$$C_{k0}(LL) = \sum_{M} (-1)^{L-M}\ (LLM-M \mid k0)\ \overline{\alpha}_{LM}(c)\ \alpha_{LM}(c)$$

If the observed distribution of radiation from the aligned nucleus is summed over the two possible polarization states of the radiation, the directional distribution function, when polarization is not considered, becomes

$$W(\theta) = \sum_{c} W(\theta c) = \sum_{k} 2(-1)^{k} C_{k0}(LL)\ P(m_i)\ (j_i j_i\ m_i - m_i \mid k0)$$

$$\times \quad W(j_f j_i\ L\ k;\ L j_i)\ D^{k}_{00}(0,\theta,0) \qquad (10)$$

To proceed to a usable formula for the angular distribution, the radiation parameter, in particular the polarization dependent part given by the α_{LM}, must be considered in further detail. To do this, it is necessary to consider a polarized wave.

The equation describing a polarized wave propagating along the 'z' axis of a Cartesian coordinate system is written

$$\underline{E} = \underline{E}_0\ e^{i(kz-\omega t)}$$

A spherical wave can be best described with the use of spherical base vectors, which are related to the triad of unit vectors of the Cartesian system by

$$\underline{\chi}_{+1} = -\frac{1}{\sqrt{2}}(\hat{i} + i\,\hat{j})$$

$$\underline{\chi}_{0} = \hat{k}$$

$$\underline{\chi}_{-1} = \frac{1}{\sqrt{2}}(\hat{i} - i\,\hat{j})$$

The spherical base vector $\underline{\chi}_{+1}$ can arbitrarily be chosen to describe the amplitude of a right circularily polarized wave of electric character and the spherical base vector $\underline{\chi}_{-1}$ will then represent a left circularily polarized wave. In general a polarization vector, denoted by $\underline{\sigma}$, can be written in terms of two components $\underline{\sigma}_1$ and $\underline{\sigma}_2$.

$$\underline{\sigma} = \underline{\sigma}_1 \hat{e}_1 + \underline{\sigma}_2 \hat{e}_2$$

The $\hat{e}_1$ and $\hat{e}_2$ are orthogonal unit vectors which are also perpendicular to the direction of motion. $\underline{\sigma}_1$ represents the component of $\underline{\sigma}$ in the $\hat{e}_1$ direction and $\underline{\sigma}_2$ gives the component of $\underline{\sigma}$ in the direction specified by $\hat{e}_2$. It is further required that $|\sigma_1|^2 + |\sigma_2|^2 = 1$. One can now express the α's in terms of $\underline{\sigma}_1$ and $\underline{\sigma}_2$.

$$\alpha_{L1}(E) = \underline{\chi}_{+1} = -\frac{1}{\sqrt{2}} (\underline{\sigma}_1 + i\sigma_2)$$

$$\alpha_{L-1}(E) = \underline{\chi}_{-1} = \frac{1}{\sqrt{2}} (\underline{\sigma}_1 - i\underline{\sigma}_2)$$

To find the corresponding magnetic multipolarities one must employ the condition that E(E) and E(M) differ in phase by $e^{i\frac{P\pi}{2}}$ where the indices refer to electric and magnetic character respectively and P is the polarization of the radiation. Thus

$$\alpha_{L1}(M) = i\,\alpha_{L1}(E) = \frac{1}{\sqrt{2}} (\underline{\sigma}_2 - i\underline{\sigma}_1)$$

$$\alpha_{L-1}(M) = -i\,\alpha_{L-1}(M) = -\frac{1}{\sqrt{2}} (\underline{\sigma}_2 + i\underline{\sigma}_1)$$

Recalling that the radiation parameter, $C_{k0}(LL)$, is proportional to the product of the α's and using the previous formulas (9) for the two types of radiation it is now possible to evaluate this product by summing over the two circular polarization states.

1. Electric radiation: $$C_k \propto \underset{L1}{\alpha}(E)\,\overline{\underset{L1}{\alpha}}(E) + \underset{L-1}{\alpha}(E)\,\overline{\underset{L-1}{\alpha}}(E)$$

$$\propto |\sigma_1|^2 + |\sigma_2|^2 = 1$$

2. Magnetic radiation: By a similar procedure, one also finds for magnetic radiation, $C_k \propto |\sigma_1|^2 + |\sigma_2|^2$

Thus when polarization is not being considered one finds that $C_{k0}(LL)$ assumes the simple form

$$C_{k0}(LL) = \sum_M (-1)^{L-M} (LLM\text{-}M \mid k0)$$

where the sum extends over the two polarization states $M = \pm 1$.

$$C_{k0}(LL) = (-1)^{L-1} (LL\ 1\text{-}1 \mid k0) + (-1)^{L+1} (LL\ -\ 1\ 1 \mid k0) \tag{11}$$

The phase relationship between the two Clebsch-Gordon coefficients is

$$(LL\ 1\ -\ 1 \mid k0) = (-1)^{2L-k} (LL\ -1\ 1 \mid k0)$$

Thus one finally gets

$$C_{k0}(LL) = (-1)^{L-1}(LL\ 1\text{-}1 \mid k0) + (-1)^{L+1+k-2L}\ (LL\ 1\text{-}1 \mid k0)$$

$$= \left\{ (-1)^{L-1} + (-1)^{k-(L-1)} \right\} (LL\ 1\text{-}1 \mid k0) \qquad (12)$$

Upon inspection of the bracketed term one finds that for odd k the term is identically zero, hence only summations over even k will occur.

Previously we had

$$W(\theta) = \sum_k (-1)^k\ C_{k0}(LL)\ W(j_f j_i\ L\ k;\ L\ j_i) \qquad (10)$$

$$\times\ P(m_i)\ (j_i j_i\ m_i\text{-}m_i \mid k0)\ D^k_{00}\ (0,\theta,0)$$

Inserting the expression for the radiation parameter into (10) and noting that the rotation matrix is related to the spherical harmonic by

$$D^k_{00}(0,\theta,0) = \frac{4\pi}{2k+1}\ Y^0_k\ (\theta 0) = \frac{4\pi}{2k+1}\ \frac{2k+1}{4\pi}\ P_k\ (\cos\theta)$$

$$= P_k\ (\cos\theta)$$

The directional distribution of gamma radiation from an aligned nucleus becomes

$$W(\theta) = \sum_{k_{even}} (LL\ 1\text{-}1 \mid k0)\ (j_i j_i\ m_i\text{-}m_i \mid k0)\ P(m_i)$$

$$\times\ W(j_f j_i\ L\ k;\ L\ j_i)\ P_k(\cos\theta) \qquad (13)$$

The Racah coefficient can be grouped with one of the Clebsch-Gordon coefficients to form a new tabulated coefficient, denoted Z_1 by Sharp (Sh 54), vizualize

$$Z_1(L\ j_i\ L'\ j_i;\ j_f\ k) = R\left\{ i^{L'-\pi'-L+\pi+k} [(2L+1)(2L'+1)(2j_i+1)(2j_i'+1)]^{1/2} \right.$$

$$\left. x\ (LL'\ 1-1 \mid k0)\ W(Lj_i\ L'\ j_i';\ j_f\ k) \right\}$$

where R denotes the "real part of" and π is zero for electric radiation and unity for magnetic radiation. Substituting the Z_1 coefficient into (13) gives

$$W_{LL'}(\theta) = \sum_{k,m_i} (-1)^a P(m_i)\ (j_i j_i\ m_i - m_i \mid k0)$$

$$x\ Z_1(L\ j_i L'\ j_i;\ j_f\ k)\ Q_k\ P_k(\cos\theta)$$

$$\text{where}\quad a = j_f + m_i + L + L' + \frac{k}{2}$$

The Q_k is a correction term to be applied because of the finite solid angle subtended by the gamma counter (Ro 53). The Z_1 coefficient (Sh 54), the Clebsch-Gordon coefficient (Se 54) and the Q_k (Da 54) have all been tabulated.

When two radiations, L_1 and L_2, are present in the transition the angular distribution becomes

$$W(\theta) = W_{L_1L_1}(\theta) + 2\ \delta\ W_{L_1L_2}(\theta) + \delta^2\ W_{L_2L_2}(\theta) \qquad (15)$$

The coefficients for different spin combinations, based on (15), have been given previously (Pr 65). The unknowns in the angular distribution formula are the population parameters and the mixing ratio. The angular distribution obtained by experiment is usually written in terms of normalized a_2 and a_4 coefficients

$$W(\theta) = 1 + a_2 P_2(\cos\theta) + a_4 P_4(\cos\theta) + \ldots \qquad (16)$$

If the number of unknowns in (13) is two or less, an experimental determination of a_2 and a_4 will, in general, be sufficient to unambiguously solve for the unknowns. It is sometimes possible to make assumptions regarding the mixing ratio and hence to reduce the number of unknowns. The comparison of the theoretical angular distributions, based on (13), for the two possible spins of the 3.62 state of Si^{29} with the measured distribution and correlation will be given in Chapter IV.

1.3 Nuclear Model Aspects

The nucleus of Si^{29} is composed of 14 protons and 15 neutrons. It might be expected, a priori, that the extreme single particle model would have some relevance in describing the spectroscopic features of Si^{29}, particularily if the nucleus of Si^{28} forms an inert core. The single neutron outside the core could then be in the $1d^3/_2$-$2s^1/_2$ shell with corresponding angular momentum assignments of $^3/_2$ and $^1/_2$ to the first two states in Si^{29}. One finds however, that the assumption of the 14 protons and 14 neutrons of Si^{28} forming an inert core is erroneus (Fr 61). Indeed states of Si^{28} exhibit collective effects which can be attributed to a permanent equilibrium deformation of the nucleus. Bromley (Br 57) has applied the single particle model to Si^{29} and finds the following discrepancies between the model predictions and experimental results.

(1) The theoretical gamma ray transition probabilities, computed by Moszkowski (Mo 54) for the single particle model are not in accord with branching ratio measurements made by Bromley.

(2) The predicted nuclear magnetic moment on the basis of the single particle model is -1.91 nuclear magnetons whereas the experimental result has been found to be -0.56 n.m. (Br 57).

(3) The experimentally determined log ft value of > 6.5 for the Beta decay of Al^{29} to Si^{29} is not explained by this model.

(4) On the basis of the single particle model, the transition from the $d^3/_2$ state to the $s^1/_2$ state is forbidden, however the experimental results obtained by Bromley indicates that an appreciable component of M1 radiation is present in the transition.

Bromley also considers the possible application of the vibrational collective model in this mass region, in particular to Si^{28}. In this model the nuclear shape is assumed to undergo vibrational oscillations about some spherical shape. Bohr (Bo 53) has shown that a level sequence of $0^+2^+(0^+2^+4^+)$ is predicted by this model and also $2<E_2/E_1<2.5$ where E_1 and E_2 are the energies of the first two excited states. Although Si^{28} has $E_2/E_1=2.5$ no evidence for the closely spaced triplet $(0^+2^+4^+)$ has yet been found.

An application of this model to Si^{29} has been made by Pandya (Pa 61). His choice of parameters for the particle-core coupling strength and the energy difference between the $d^3/_2$ and $s^1/_2$ states yields reasonable values for the energy spectrum of the low-lying states of Si^{29}, however there is poor agreement with experimental results with regard to the nuclear magnetic moment of Si^{29} and the log ft value for the Beta decay of Al^{29} to Si^{29}. Thus it appears that neither the single particle nor the vibrational collective models are particularily relevant in describing nuclei in the mass region of A=28. It has been previously mentioned that Si^{28} possesses a permanent deformation which would give rise to collective effects. Litherland (Li 58) has made a thorough study of the mirror nuclei Al^{25} and Mg^{25} and has ascertained that the low-lying levels in these nuclei are of a rotational origin.

A study of P^{29}, the mirror nucleus of Si^{29}, has been carried out in this lab (Da 65) using the reaction $Si^{28}(d,n)P^{29}$. The results indicate that the Nilsson generalized single particle model best explains the spectroscopic features of P^{29}.

This model has been applied to P^{31} (Da 65)' and although the rotational -particle coupling is appreciably weaker than in the A=25 system, there is sufficient evidence to support rotational collective behavior up to A=31.

Rakavy (Ra 57) has suggested that nuclei in the $d^5/_2$ shell will exhibit rotational characteristics, the strength of the rotational- particle coupling being most prominent in the middle of the shell. This would embrace nuclei in the mass region from A=16 to A=28. Thus it appears reasonable that Si^{29} should exhibit rotational behavior with intermediate strength particle-core coupling. Before applying this model to Si^{29}, the energy level diagram fig 1.1, illustrates the known spectroscopic features of the lower energy levels of Si^{29}.

Strong evidence supporting the rotational model is given by the branching ratio measurement (Br 57) on the 2.03 Mev level which decays by a direct ground state transition and also via the 1.28 Mev level. The latter transition involves an E2-M1 mixture, the former is pure E2. Experimental results (Br 57) reveal that approximately 99% of the decay is directly to ground state. The rotational model predicts E2 enhancement for transitions between members of the same band. A diagram of the energy levels of the Nilsson model (Ni 55) is given in figure 1.2 and illustrates the levels as a function of the spheroidicity (departure from spherical shape).

Two quantum numbers which are employed in this model are denoted by K and Ω where K is the projection of the total angular momentum on the nuclear symmetry axis and Ω is the projection of the intrinsic particle angular momentum on this axis. The model assumes a permanent, symmetrical

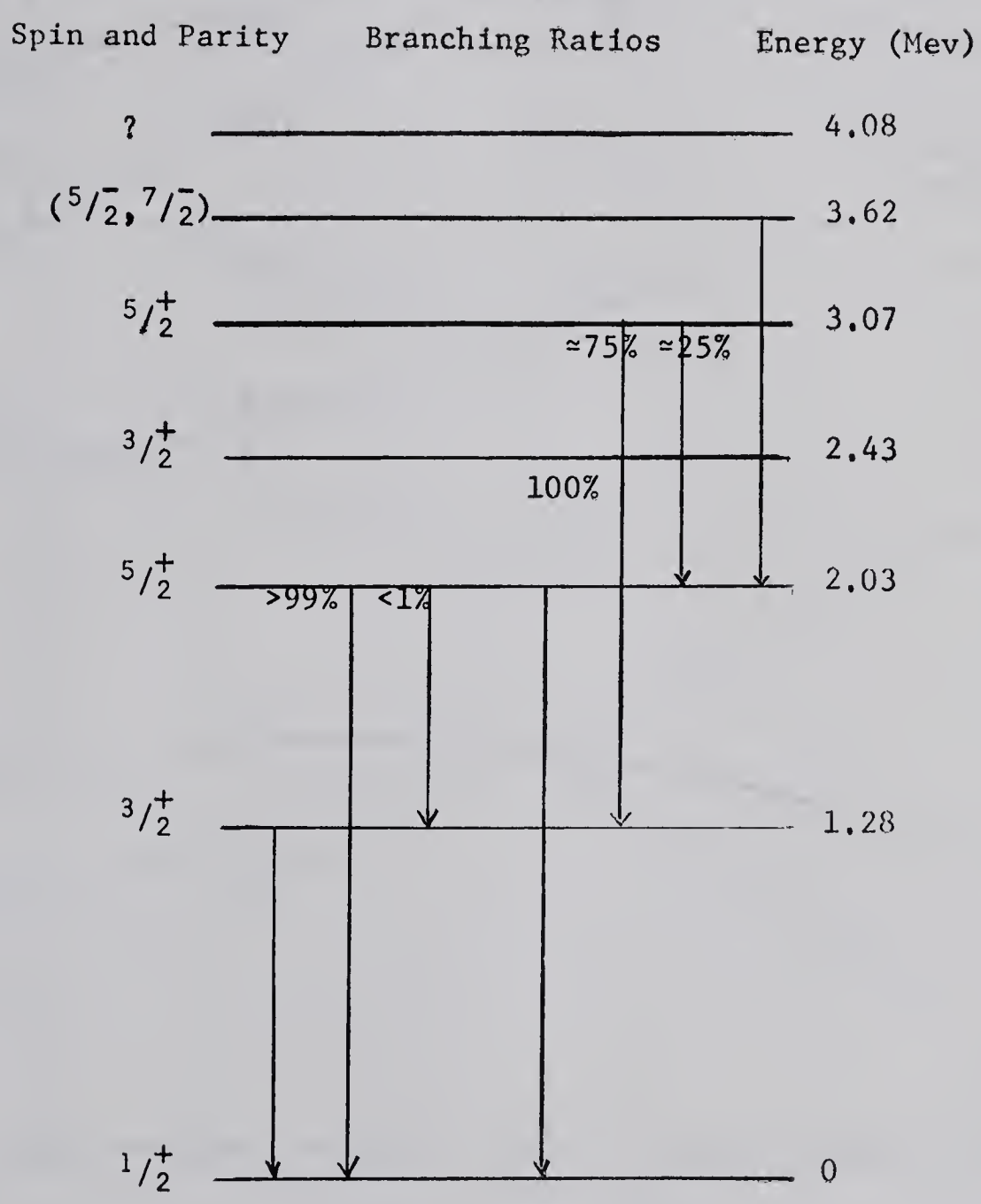

Fig. 1.1 The Low Lying Energy Levels of Si^{29}

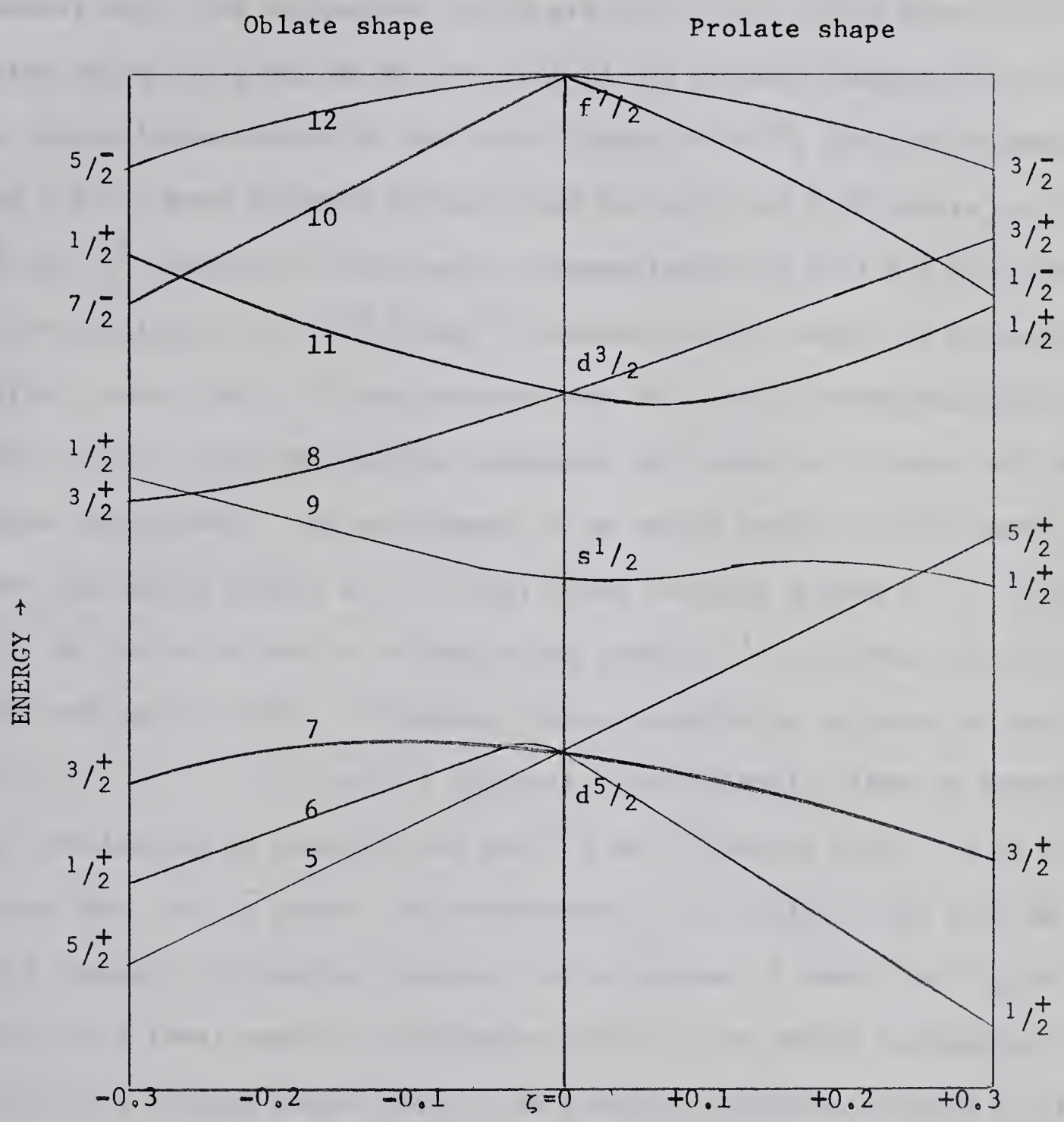

Fig. 1.2. Energy levels of the Nilsson model as a function of ζ for d-s shell nuclei. The single particle states upon which the numbered Nilsson orbits are based, are given on the ζ=0 axis (Ni 55).

nuclear distortion, denoted by ζ, and the aspects are manifested in the rotational motion of the entire nucleus about an axis perpendicular to the symmetry axis. The collective levels are then built on the single particle states which are given on the ζ=0 axis of the Nilsson diagram, fig. 1.2. Two possibilities exist for the lower levels of Si^{29}; the ground state defines a $K=^1/_2$ band (Nilsson orbit 9) and the 1.28 and 2.03 levels are the $^3/_2^+$ and $^5/_2^+$ members of this band - alternatively the 2.03 and 2.43 levels can be considered as the $^5/_2^+$ and $^3/_2^+$ members of the band. The latter possibility leaves the 1.28 level as the base for a $K=^3/_2$ rotational band (Nilsson orbit 8). The two possible sequences correspond to prolate and oblate shapes respectively. The assignment of an oblate shape to Si^{29} leads to the first odd parity state, at 3.62 Mev, being assigned a spin of $^7/_2$ (see fig. 1.2). On the other hand a prolate shape predicts $^1/_2$ for the spin of the first odd parity state. If however, the spheroidicity is positive and small ($\zeta<0.1$), the $^1/_2^-$, $^3/_2^-$, and $^5/_2^-$ states are sufficiently close in energy so that overlapping is possible and the $^3/_2^-$ or $^5/_2^-$ states could lie at a lower energy than the $^1/_2^-$ state. The measurement of the spin of the 3.62 Mev level could possibly distinguish between the two shapes. A result of $^7/_2$ for the spin of the level would be conclusive proof for an oblate assignment to Si^{29} since for a prolate shape there is no possible mechanism whereby a spin of $^7/_2$ would appear before the lower spin states. On the other hand a result of $^5/_2$ for the spin of the 3.62 Mev state, while still favoring an oblate shape, would not be conclusive if the spheroidicity is small. Bromley (Br 57) presents some evidence which indicates, but does not confirm, an oblate shape for Si^{29} with $\zeta\simeq-0.15$. One exception to the evidence favoring an oblate assignment is the previously mentioned branching ratio of the 2.03 Mev

state which decays predominately to the ground state. This discrepancy for an oblate shape can be removed if one considers band mixing (Ma 61) in which case a term of the form $-\hbar/2\mathcal{J} \times J \cdot j$ is added to the rotational Hamiltonian. Here J and j are the respective angular momenta of the core and single particle and $\mathcal{J}$ is the moment of inertia of the core. This operator connects bands where $\Delta K=1$ (and also connects two $K=^1/_2$ bands). In the case of an oblate assignment to Si^{29} the operator would mix the states originating from the $K=^1/_2$ band, based on the ground state, with the states of the $K=^3/_2$ band, based on the 1.28 level.

In summary, the nucleus Si^{29} is best described by a collective model with rotational like behavior and which appears to have it's greatest applicability to the A=25 system with relevance up to, at least, A=31. The core, composed of 14 protons and 14 neutrons, has a permanent, symmetrical deformation. Experimental evidence indicates that the spheroidicity is negative which implies oblate shape. The single neutron then moves in the field of the core and the various states originate from the rotational core-particle coupling.

CHAPTER II

2.1 Experimental Equipment and Procedure

(a) Accelerator and Target Room

The 6 Mev Van de Graaff electrostatic accelerator, located at the Nuclear Research Centre, University of Alberta, was used to accelerate the alpha particles which initiated the $Mg^{26}(\alpha,n\gamma)Si^{29}$ reaction. The beam energy is stabilized by means of slits which are located immediately following a 90° analyzing magnet. The slits are connected to a corona stabilizer near the upper terminal of the accelerator, the slit signals controlling the corona drain from terminal to ground. The analyzed beam then passes through the straight-through port of a switching magnet (used for slight steering of the beam), and a quadrupole lens which acts as a focusser. Definition of the beam is obtained from vertical and horizontal slits which follow the lens, and a lead collimator placed approximately one foot from the target. The target itself is located in an aluminum target chamber and can be varied in height and angle. The target chamber is positioned over the centre of a correlation table, upon which the detectors are placed. Angular detector positions, in steps of 15°, have been marked on the table. Figure 2.1 illustrates the experimental apparatus which is located in the target room.

(b) Detectors

The neutron detector used in this experiment is a liquid scintillator type*, of dimensions $1^1/_2$" in diameter and length, and is mounted on a Phillips 56-AVP photo-multiplier. This detector has three outputs, a fast output, a linear output, and a pulse shape discriminator output, the latter producing an output pulse only for incident neutrons.

* Model NE-5553B Nuclear Enterprises, Winnipeg Man.

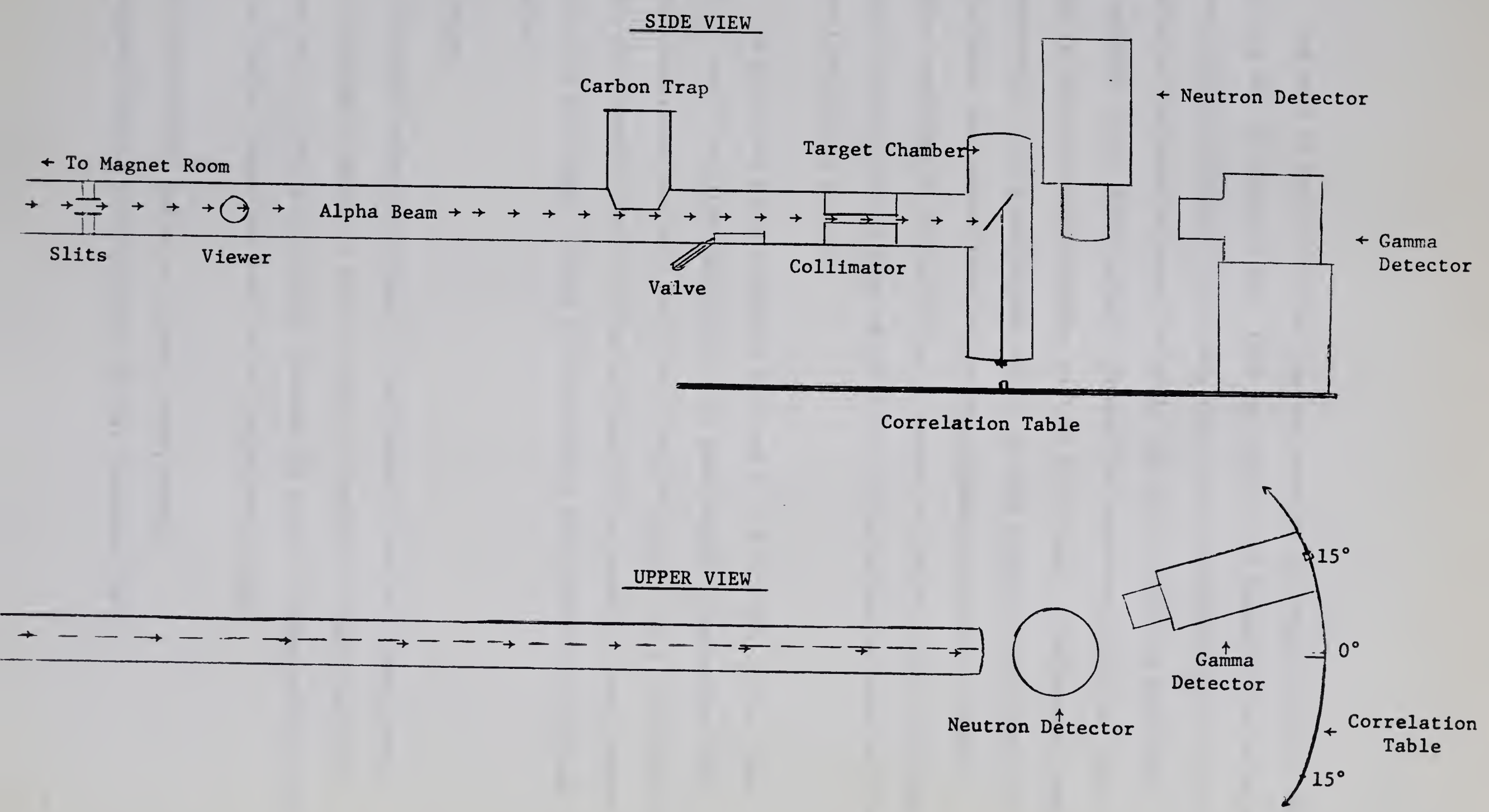

Figure 2.1 Target Room Equipment

The axis of the cylindrical neutron detector is perpendicular to the beam axis and is located 6 cms. from the target. The height of the midpoint of the liquid scintillator is 25 cms. above the correlation table. The positioning of the detector above the table was done in order to facilitate the movement of the gamma detector through two quadrants, hence any anisotropy in the angular distribution pattern due to table misalignment, would be observable. Within statistical error, no such anisotropy was found. In this scheme, the neutron detector intercepts gamma radiation for gamma detector positions of 0° and 15°, with respect to the beam axis, and attenuation correction factors must be applied to the experimental data for these angles (Corrections 2.2-b).

The principal gamma detector* used was a 3" by 3" NaI crystal coupled to a 54-AVP Phillips photo-tube. Also used during a gamma-gamma coincidence measurement was a 2" by 2" NaI crystal** mounted on a 8S8 photo-tube. For all experimental runs the front surfaces of the detectors were located 15 cms. from the target. Figure 2.1 illustrates the correlation table and detectors.

(c) Targets

Two Mg^{26} targets were used in the course of the preliminary runs; one of loading 90 ugms./cm^2. and the other of loading 200 ugms./cm^2. Both targets had a 0.005" gold backing. Because the yield of gamma radiation was low the thicker target was used for all experimental runs.

* Model "Scintibloc" Quartz et Silice, Paris, France.

** Harshaw Integral Line Detector, BS-454, Cleveland, Ohio

(d) Electronics

(i) n-γ Coincidence

Only gamma radiation in coincidence with neutrons is counted, the incident alpha beam specifying a reference axis. The electronics associated with the n-γ coincidence are shown in figure 2.2.

The circuits which carry the gamma and neutron pulses to be analyzed are designated by S_g and S_n. Each system contains a pre-amplifier coupled to a double-delay line amplifier. The bi-polar output pulses from the amplifiers are delayed by variable delay lines* which are adjusted so that the slow pulses arrive at the input of a multi-channel analyzer (kicksorter) within the time duration of a gate pulse generated by the fast coincidence system. In this experiment a 1024 channel, two parameter, pulse height analyzer** was used. The kicksorter was programmed in the 2×512 mode, so that the gamma spectrum to be analyzed was fed into the first 512 channels, unit A, and the neutron spectrum into the second 512 channels, unit B.

In the fast coincidence channel, a time to amplitude converter (TAC) receives limited and amplified pulses which originate from the last dynodes of the two detectors, labelled F_g and F_n in figure 2.2. The essential element of the TAC is a 6BN6 gate tube which has two input grids. The amplitude of the output pulse from the converter depends on the time overlap of the two grid signals. The output signal is then fed into a single channel

* Type 2011, AD-YU Electronics Ltd. Passaic N.J.

** Model CN-1024, Technical Measurement Corp. North Haven, Conn.

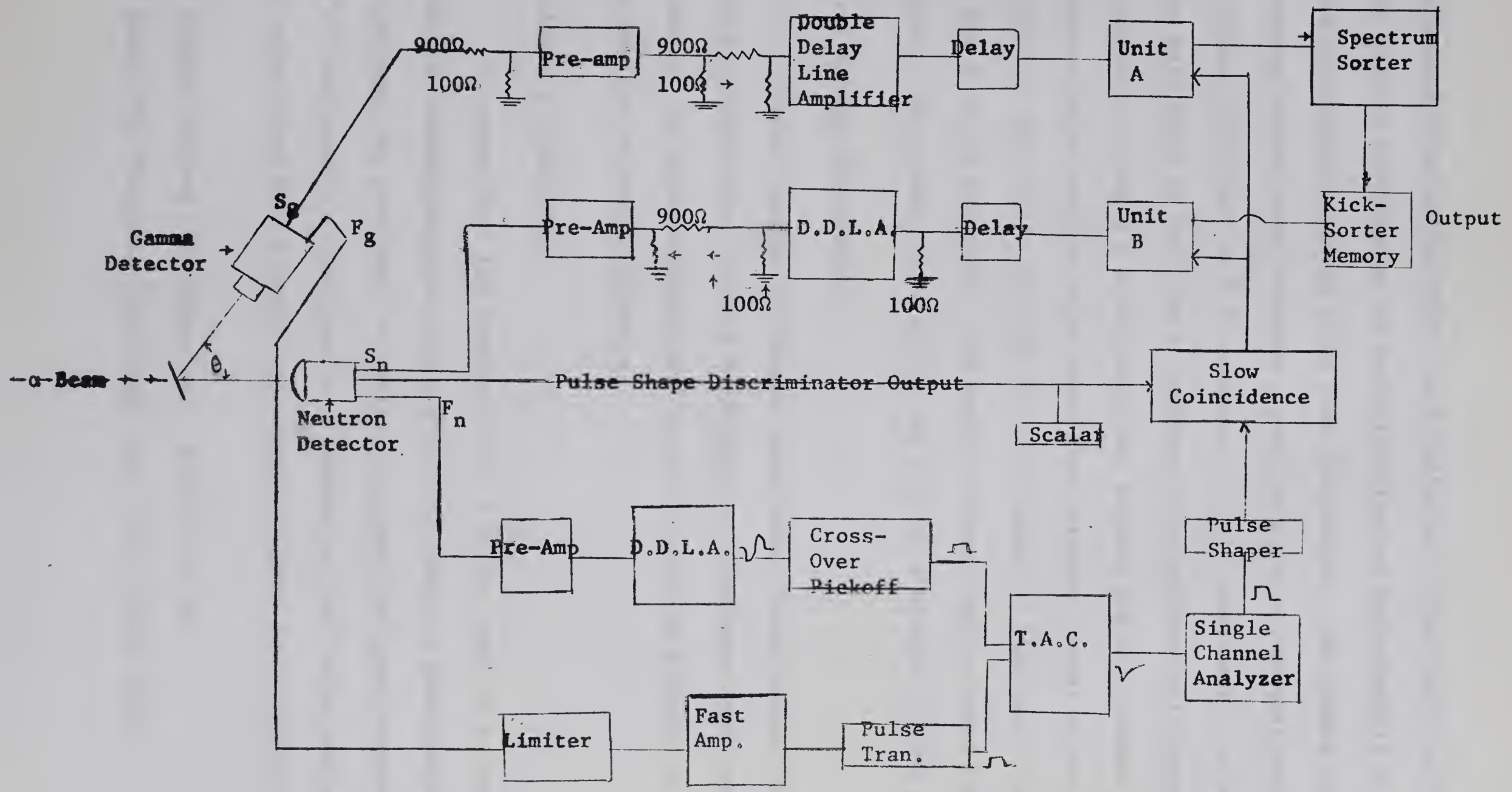

Fig. 2.2 Electronics for n-γ Coincidence Experiment

analyzer* whose window width can be adjusted to the resolving time desired. For the n-γ coincidence the resolving time was approximately 40 nano-seconds. The discriminator output pulse from the analyzer then passes through a pulse shaping circuit which produces a positive pulse of 10 volts amplitude and variable width (set at 2.4 u-seconds for this experiment). To ensure that the gate pulse is only due to neutrons in coincidence with gamma rays it is necessary to demand a slow coincidence between the fast channel and the neutron pulse from the pulse shape discriminator circuit of the neutron detector. The output from the slow coincidence is then used to gate units A and B of the kicksorter. The neutron pulses from the pulse shape discriminator were counted by a scalar and used as a monitor for the experiment.

(ii) Angular Distribution

A direct angular correlation experiment, termed angular distribution, was also undertaken. In this experiment no coincidence requirements are imposed on the gamma radiation and the fast system is disabled by setting the kicksorter to anti-coincidence.

(iii) γ-γ Coincidence

To ensure that the feeding of the 3.62 Mev level is by neutrons only, and not cascade radiation from the 4.08 Mev level, a gamma-gamma coincidence experiment was performed. For this coincidence the gamma spectrum from the 3"×3" NaI crystal is analyzed by a spectrum sorter** which can be programmed to select from 1 to 8 bands, set around the gamma photo-peaks of interest.

* General Purpose Coincidence Unit, EB-5076, (Go 60)

** Model 245, Technical Measurement Corp. North Haven, Conn.

The coincident gamma radiation, detected by a 2"×2" NaI crystal, are routed into the appropriate bands depending on the photo-peak with which this radiation is in coincidence.

For the γ-γ coincidence the neutron detector is replaced with the 2"×2" gamma detector. The pre-amplifier, double-delay line amplifier, and the cross-over pick-off in the fast neutron channel of figure 2.2 are replaced by a limiter and amplifier. The spectrum sorter was programmed in a 2×512 mode so that gamma radiation coincident with the 1.59 Mev and 2.03 Mev gamma radiation would fall into the first or last 512 channels of kicksorter memory, respectively. The two gamma detectors were located in different quadrants, both at 90° with respect to the incident beam direction.

The results of the γ-γ coincidence are presented in the preliminary results (3.1 b). A γ-γ correlation, in which one of the gamma detectors would be varied in angular position, was not attempted.

During all of the coincidence runs an oscilloscope was used for monitoring purposes to ensure that the pulses to be analyzed by the kicksorter arrived within the time duration of the gate pulse, and also that any electronic malfunctions would be immediately detectable.

2.2 Reaction Considerations

(a) Kinematics

The kinematics for the $Mg^{26}(\alpha,n\gamma)Si^{29}$ reaction have been computed for incident alpha energies from 5.2 Mev to 5.8 Mev. The following table, 2.1, gives the energies of the neutrons, in the forward direction, which feed the residual states in Si^{29} up to 4.08 Mev.

Low Lying Energy (Mev) Levels of Si^{29} ↓	Alpha Energy (Mev) → 5.2	5.3	5.4	5.5	5.6	5.7	5.8
Ground	5.03	5.13	5.23	5.32	5.43	5.52	5.61
1.28	3.70	3.80	3.89	3.99	4.08	4.18	4.28
2.03	2.91	3.00	3.10	3.20	3.29	3.39	3.49
2.43	2.48	2.58	2.68	2.77	2.87	2.97	3.06
3.07	1.79	1.89	1.99	2.08	2.18	2.28	2.38
3.62	1.18	1.28	1.38	1.48	1.58	1.68	1.78
4.08	0.65	0.76	0.86	0.96	1.06	1.17	1.27

Table 2.1 Neutron Energies in the Forward Direction

The kinematics of competing reactions have also been considered. For the other two isotopes of Magnesium, Mg^{24} with 80% natural abundance and Mg^{25} with 10% natural abundance, the Q values for a (α,n) reaction are -7.2 Mev and +2.7 Mev, respectively. Only the $Mg^{25}(\alpha,n)$ reaction is possible at the alpha energies encountered in the present experiment, however no yield from this reaction was seen.

In the angular distribution experiment, the reaction $Mg^{26}(\alpha,p)Al^{29}$, with a Q value of -2.86 Mev, could contribute a 1.40 Mev gamma ray for a ground state transition from the first excited state in Al^{29}. No such transition was observed.

Due to Carbon buildup on the target, the inelastic scattering reaction $C^{12}(\alpha,\alpha')C^{12}$ is possible. This scattering process yields a prominent gamma ray of 4.43 Mev energy and will contribute to the background of the angular distribution runs. The Carbon buildup is minimized by a Carbon trap which is located near the target (fig. 2.1).

(b) Corrections

(1) Gamma ray attenuation by the neutron detector

This correction must be applied to the n-γ correlation when the gamma detector is located at 0° or 15°. The intensity of gamma radiation, with the neutron detector in and out of position, was measured both during the experiment and also with a radio-active source, Na^{22}. The following correction factors, table 2.2, were found for the prominent gamma rays observed in the reaction.

E_γ (Mev)	0° Correction	15° Correction
1.28	1.14	1.08
1.59	1.12	1.05
1.79	1.11	1.04
2.03	1.10	1.02
2.43	1.07	1.02

Table 2.2 Correction Factors

(11) Solid angle corrections

Since the gamma detector occupies a finite solid angle, a correction must be applied to the measured distribution and correlation. The theory for the solid angle corrections has been considered by Rose (Ro 53), who has denoted the correction factors by Q_k. Tables of Q_k for different source to detector distances, and different gamma ray energies, have been given by Davisson (Da 54) and Yates (Ya 65).

The Q_k are defined by;

$$Q_k = \frac{\int_0^\pi P_k(\cos\theta)\xi(\beta)\sin\beta d\beta}{\int_0^\pi P_0(\cos\theta)\xi(\beta)\sin\beta d\beta}$$

where β is the angle between the propagation direction of the gamma ray and the crystal axis, and $\xi(\beta)$ is the efficiency of the gamma detector in detecting this gamma ray.

Table 2.3 lists the relevant Q_k for a source to detector distance of 15 cms.

	Gamma Energy (Mev)→				
	1.28	1.59	1.79	2.03	2.43
Q_2=	0.97	0.97	0.97	0.97	0.97
Q4=	0.90	0.90	0.90	0.90	0.90

Table 2.3 Solid Angle Corrections

CHAPTER III

3.1 Preliminary Results

(a) Yield

The 3.62 Mev state in Si^{29} is first excited for an incident alpha energy of 4.1 Mev. Litherland (Li 60) has measured the yield of the 1.59 Mev radiation which is emitted from this state, for alpha energies from 5 Mev to 5.3 Mev. His yield curve for the 1.59 Mev gamma ray is compared with the result obtained in the present experiment, which covered the range of incident alpha energies up to 5.5 Mev, in figure 3.1. Both curves show a resonance at about 5.23 Mev, and in addition, the present experiment indicates a further resonance corresponding to a bombarding energy of 5.51 Mev.

In figures 3.2 and 3.3, singles spectra taken at the two resonance points are given.

(b) Gamma-Gamma Coincidence

At both resonances, the 4.08 Mev state is excited and it is necessary to ascertain if this state de-excites to the 3.62 Mev state by the emission of a 0.46 Mev gamma ray. A strong cascade transition between the two levels could disturb the n-γ correlation of the 1.59 Mev radiation If the 1.59 gamma ray originated from such a cascade, it would be analyzed as a valid coincidence with the neutron feeding the 4.08 Mev level.

The γ-γ coincidence measurement was performed with the circuitry described in section 2.1 (d), (111).

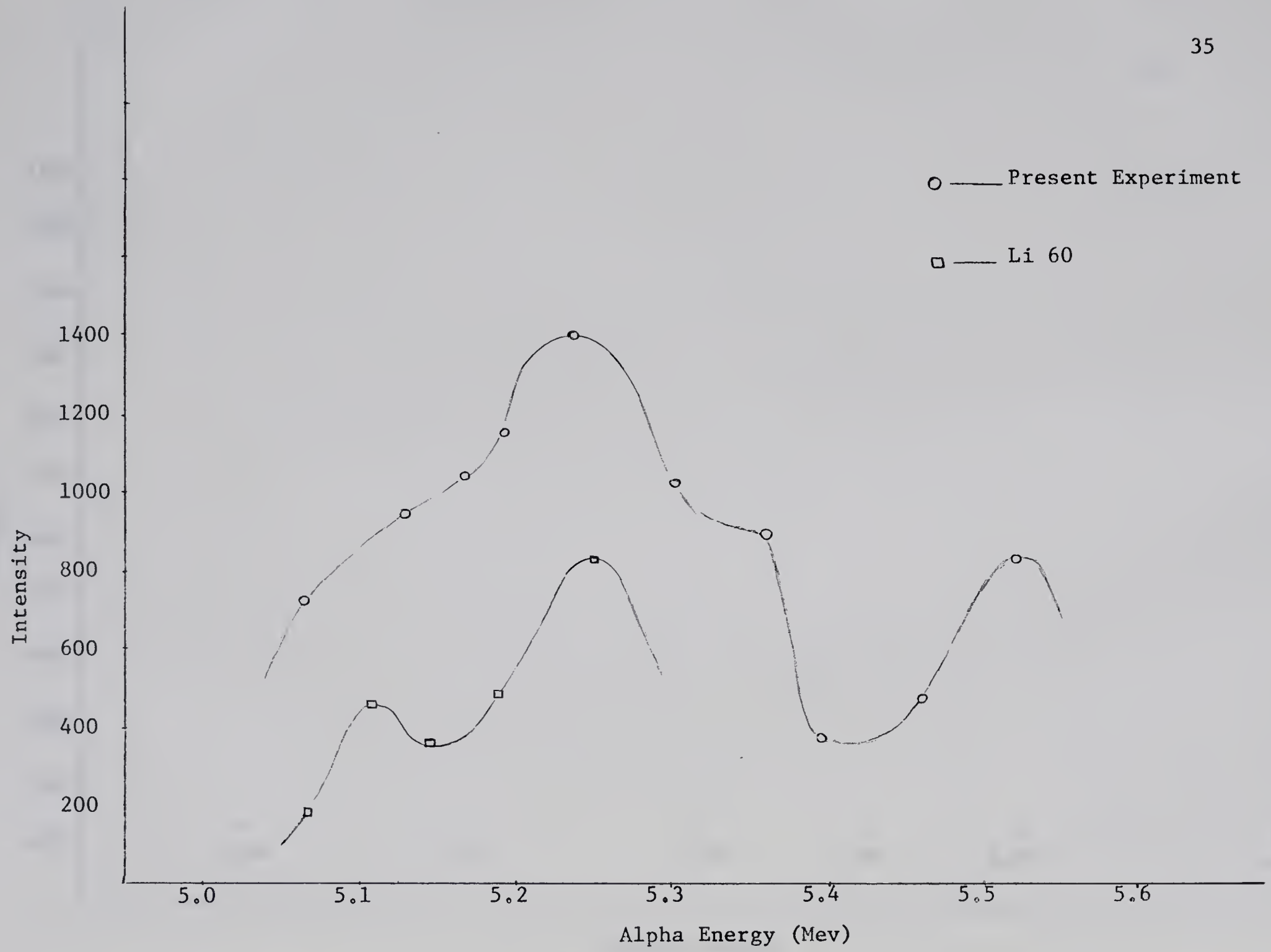

Fig. 3.1 Yield of 1.59 Mev Gamma Ray

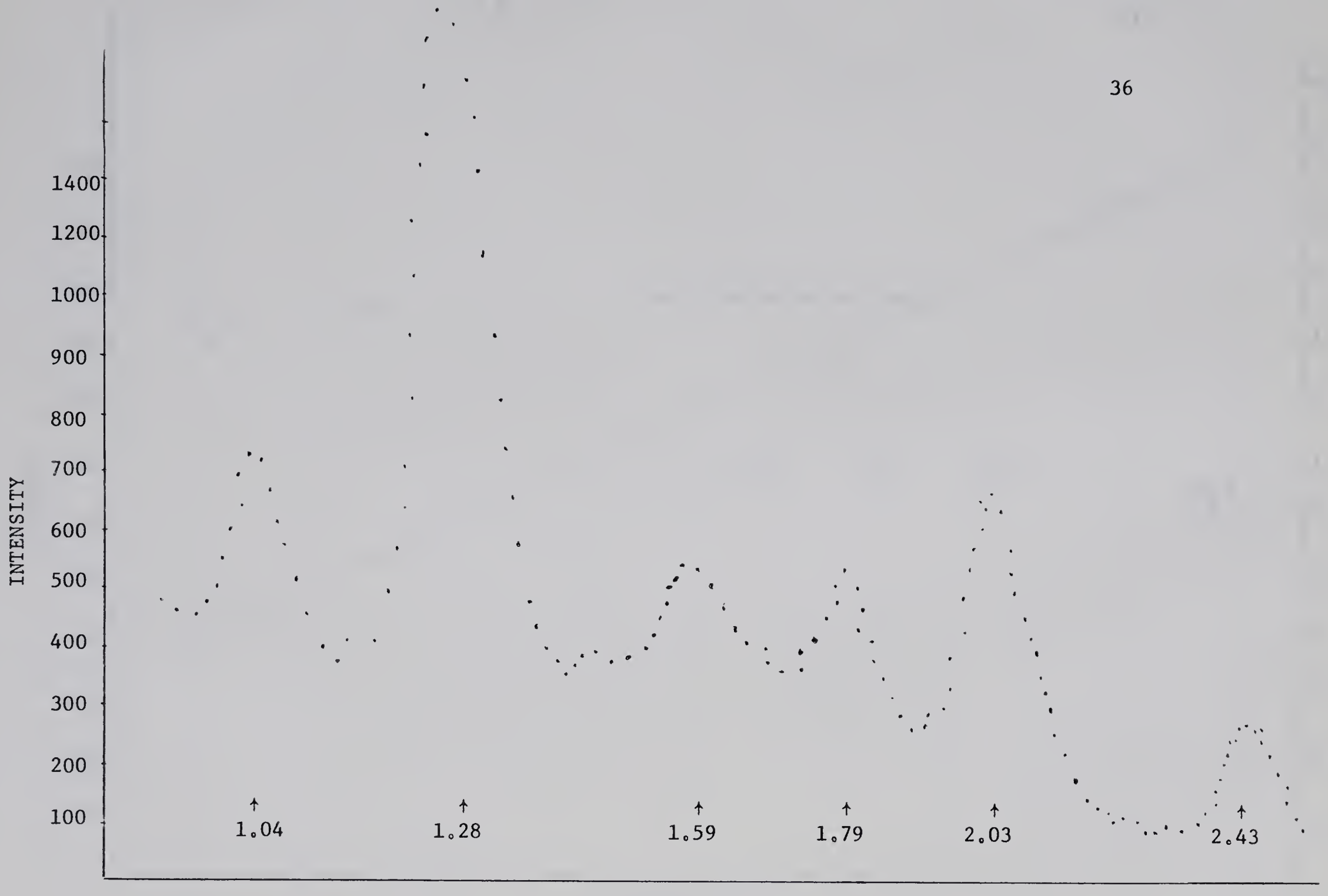

Fig. 3.2 Singles Spectrum for E_α=5.23 Mev

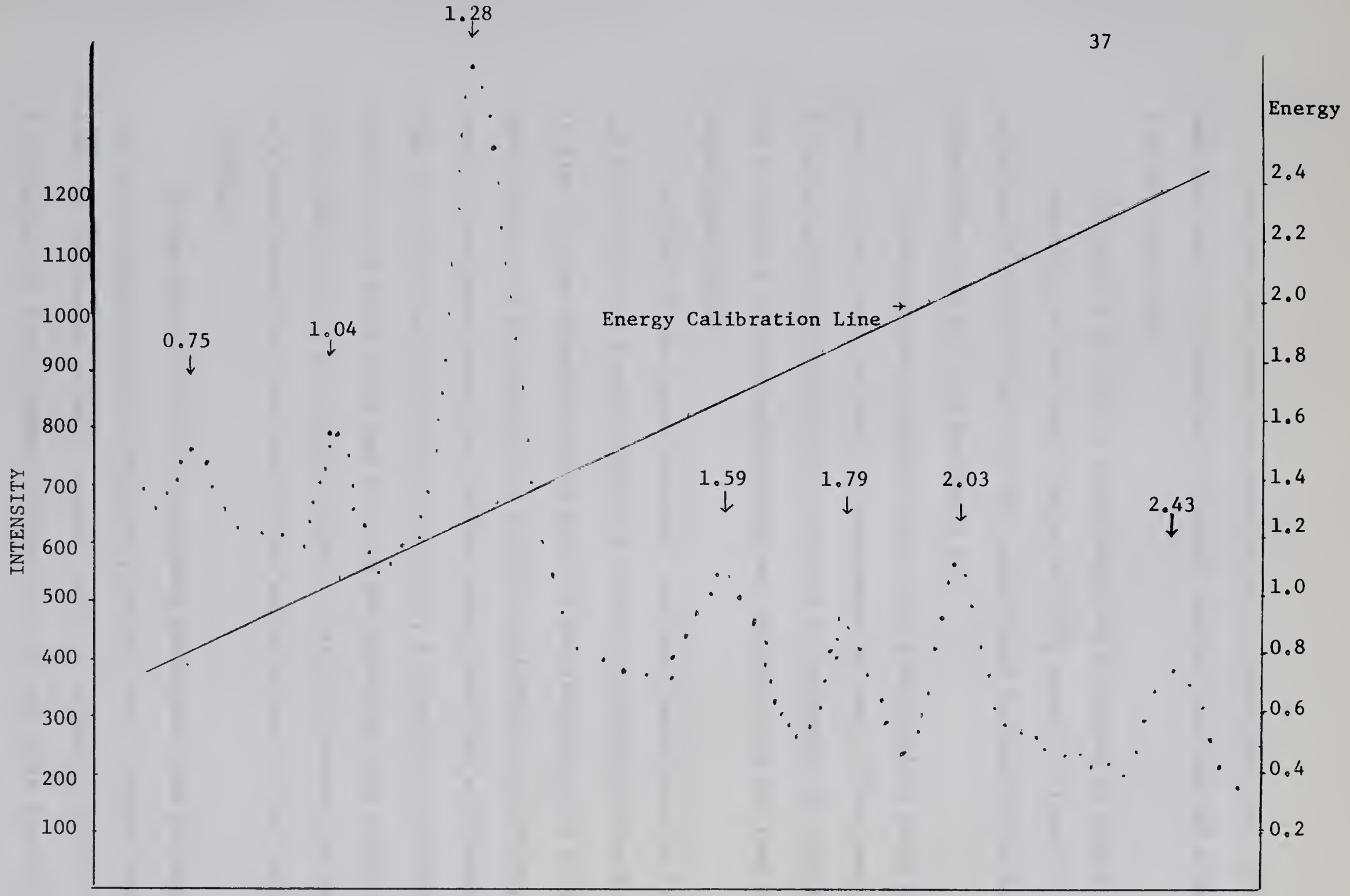

Fig. 3.3 Singles Spectrum for E_α=5.51 Mev

The spectrum sorter was used to set a gate around the 1.59 Mev photo-peak and also, for comparison purposes, another gate was set around the 2.03 Mev photo-peak.

The results of the γ-γ measurement are presented in figure 3.4.

Referring to the level diagram of Si^{29}, shown in figure 3.5, gamma radiation of 1.04 Mev and 1.59 Mev energy would be expected to be in time coincidence with the 2.03 Mev gamma ray.

The experimental results, figure 3.4, show distinct peaks at 1.04 Mev, 1.28 Mev, and 1.59 Mev. The appearance of the 1.28 Mev peak is due to a random coincidence, which was confirmed by performing an experimental run in which a 180 nano-second delay was inserted into the fast neutron coincidence channel.

In the 1.59 Mev gated spectrum, prominent peaks occur at 1.28 Mev and 2.03 Mev, with a small peak at 0.75 Mev. The weak 0.75 Mev transition is also in time coincidence with the 1.59 Mev radiation. The 1.28 Mev peak again appears as the result of a random coincidence. In addition, since the 0.75 Mev gamma feeds the 1.28 Mev state, which has a lifetime shorter than the resolving time of the electronics, a true time coincidence between the 1.59 gated gamma and the 1.28 Mev gamma ray also occurs. No distinct peaks occur in the energy region of 0.46 Mev; however the possibility of a weak transition from the 4.08 Mev state to the 3.62 Mev state is not excluded.

On the basis of the γ-γ coincidence measurement one can ascertain that the intensity of 1.59 radiation produced from a cascade transition from the 4.08 state is small compared with the intensity of 1.59 radiation originating from neutrons feeding the 3.62 Mev state from Si^{30}.

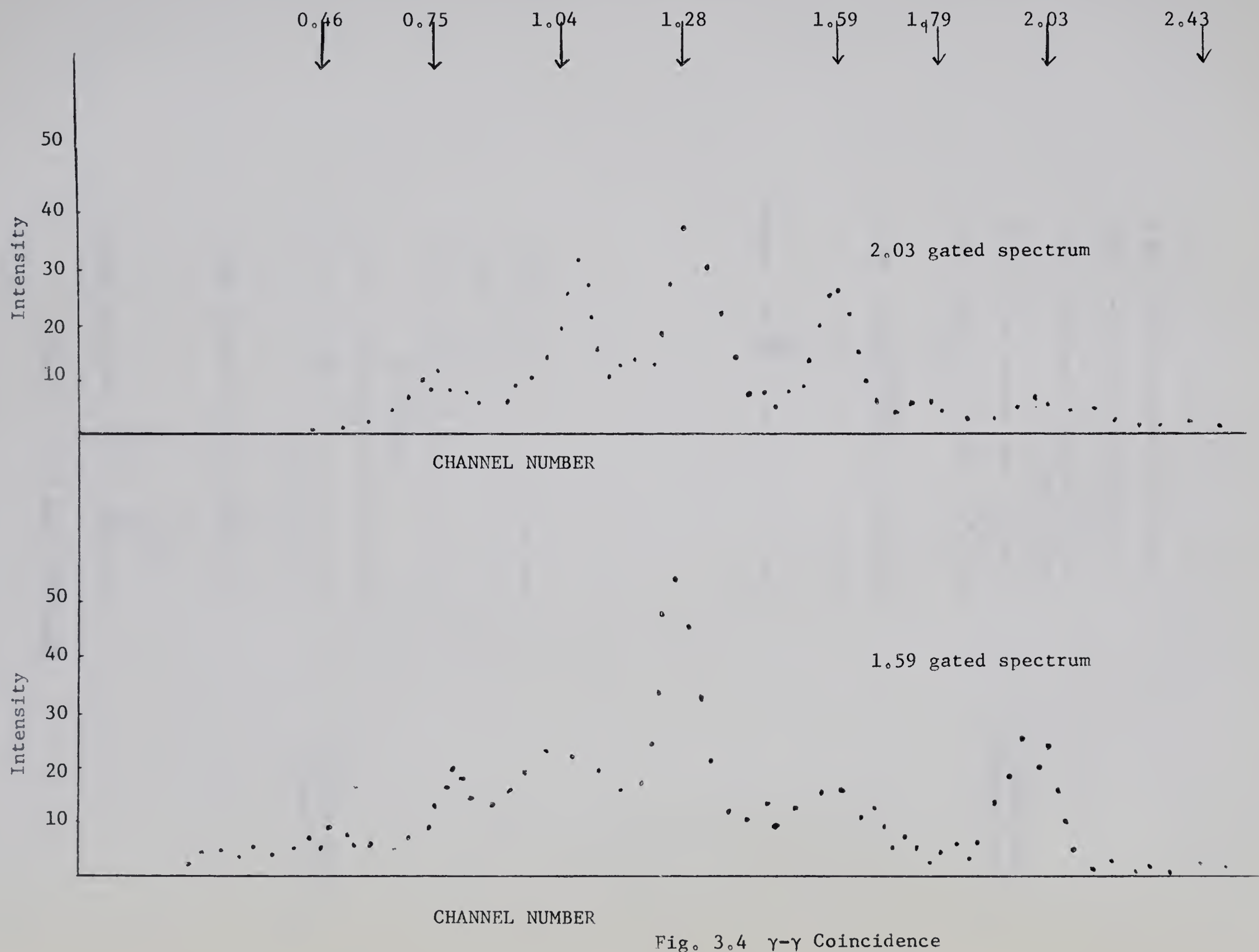

Fig. 3.4 γ-γ Coincidence

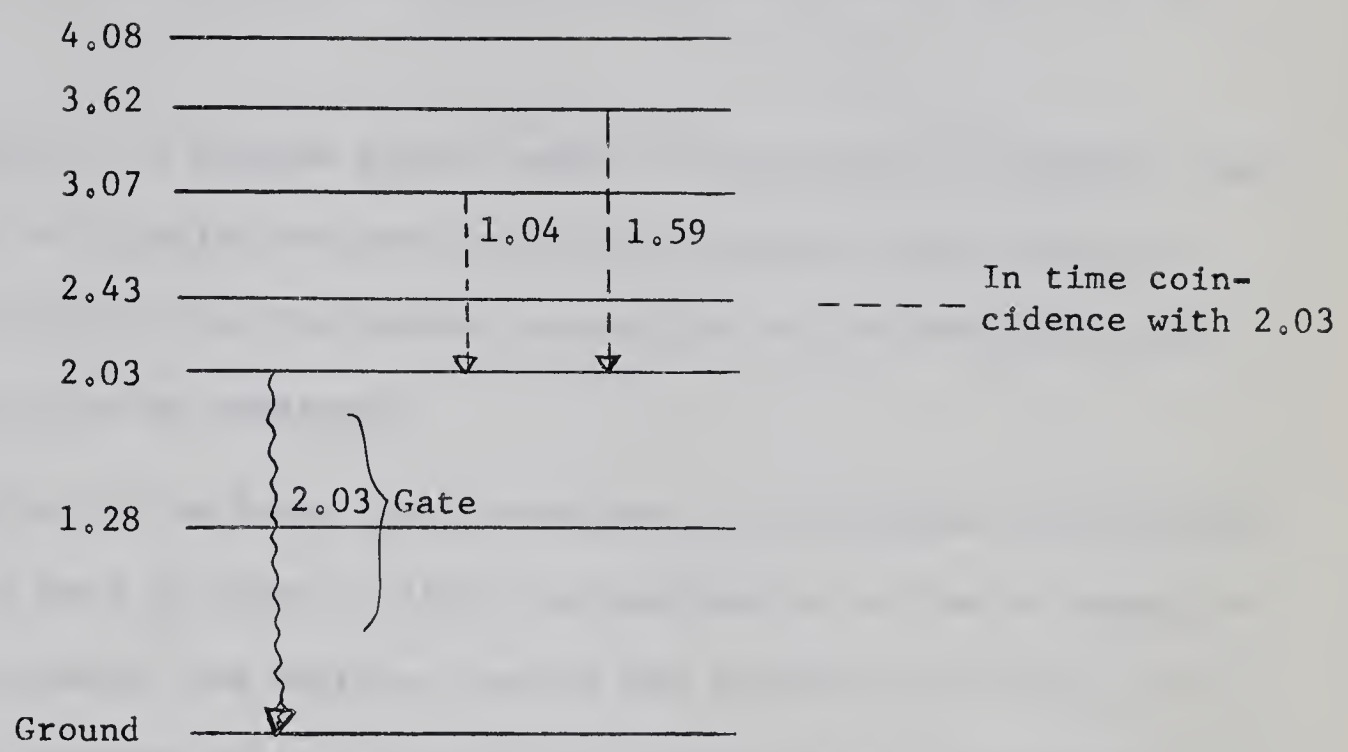

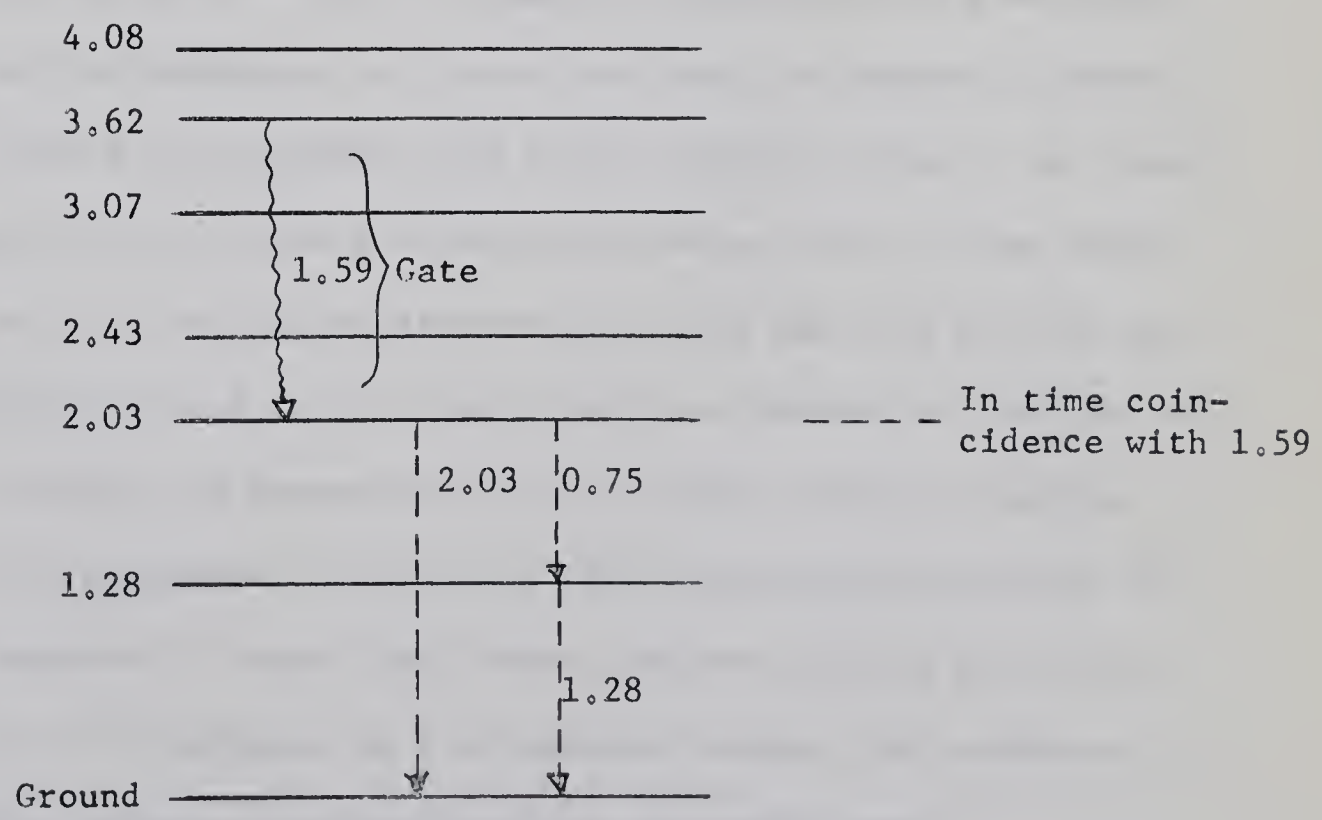

Fig 3.5 2.03 and 1.59 Gates

In figure 3.6 a typical gamma ray singles spectrum from the angular distribution is shown. The angular distribution was run at the 5.23 Mev resonance.

In figure 3.7 a neutron gated, gamma ray spectrum is presented. The neutron-gamma correlation was performed at an incident alpha energy of 5.51 Mev. The reasons for the running points for the two experiment are given in the following paragraph.

The choice of the lower alpha resonance for the angular distribution experiment was made in order to limit the neutrons to as low an energy as possible. In general, the neutrons feeding the states in Si^{29} will not be pure wave and mixtures will be present. For example, a 2^+ resonance in Si^{30} (which Litherland assumes feeds the low-lying positive parity states in Si^{29}) will decay to the 3.62 Mev residual state in Si^{29} with the emission of p-wave neutrons and possibly an admixture of f-wave neutrons. For pure p-wave neutrons, only the $m=\pm 1/2, \pm 3/2$ magnetic substates could be populated, however with an admixture of f-wave neutrons, the magnetic substates up to $m=\pm 7/2$ could be populated. Low energy neutrons carry a low angular momentum and for E_α=5.23 Mev the neutrons feeding the 3.62 Mev state have an energy of 1.23 Mev in the forward direction and only 0.9 Mev energy in the direction normal to the beam direction. Because of the low neutron energies involved, an assumption of pure p-wave neutrons feeding the 3.62 Mev state is reasonable. A spin of 3^- for the compound state of Si^{30} would entail a mixture of s-wave and d-wave neutrons feeding the 3.62 Mev state, but as for a 2^+ resonance in the compound nucleus, the admixture of the higher angular momentum neutrons would be extremely small.

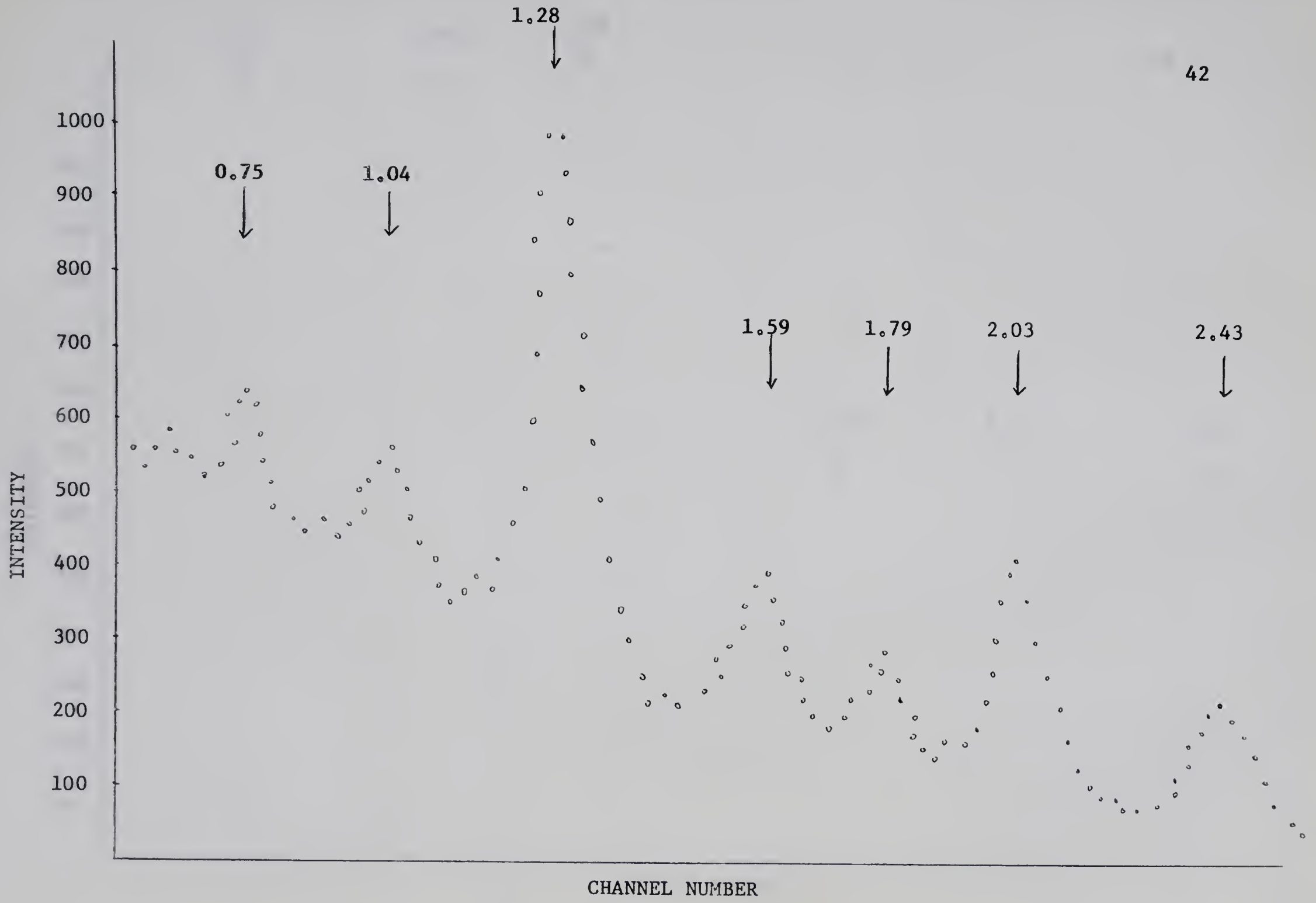

Fig. 3.6 Gamma Ray Singles Spectrum with E_α=5.23 Mev

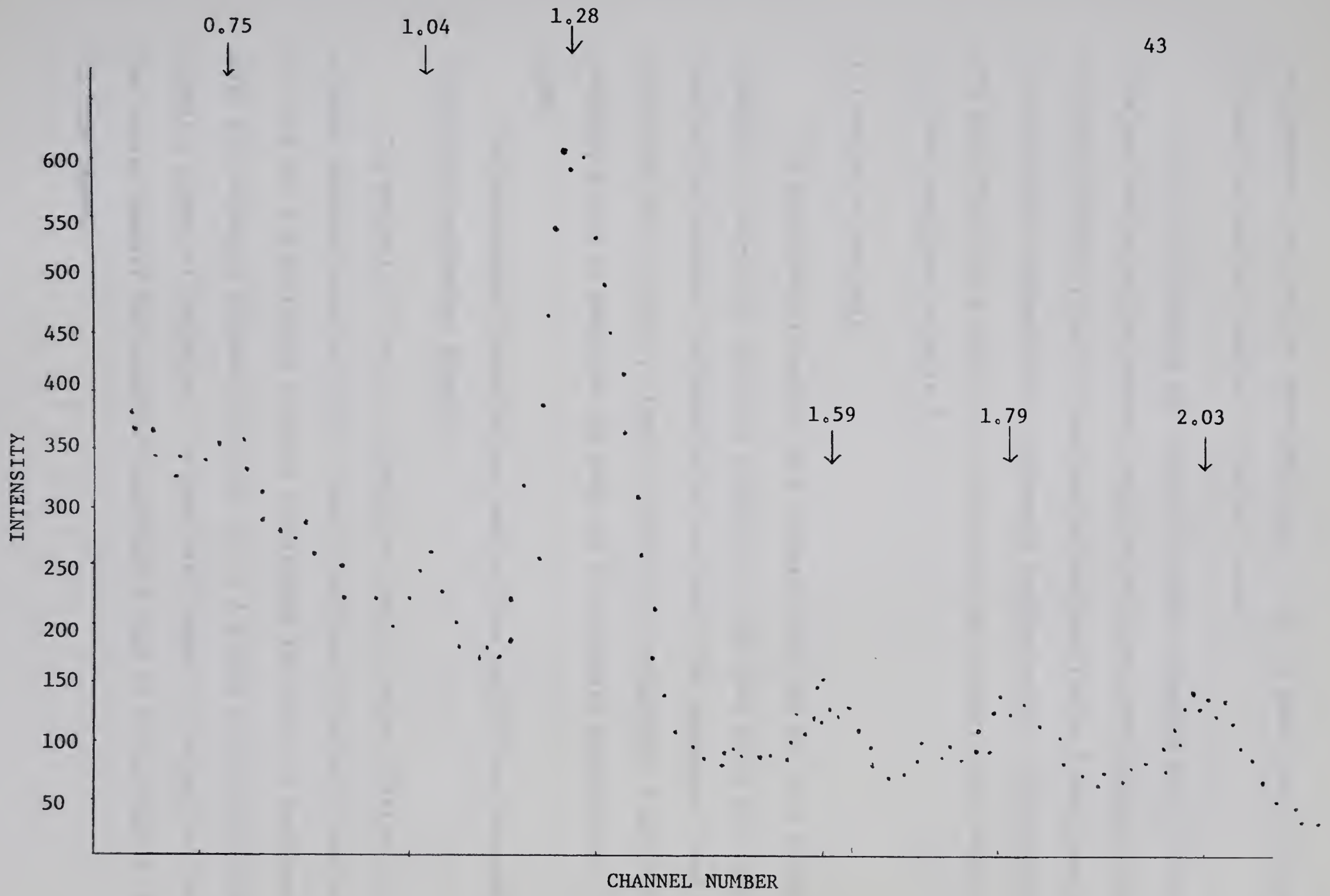

Fig 3.7 Neutron Gated Gamma Ray Spectrum, E_α=5.51 Mev

The angular distribution experiment was run at the lower alpha resonance to keep the neutron energies as low as possible.

The n-γ correlation was run at the alpha resonance at 5.51 Mev. This was done since the neutron detector efficiency now becomes relevant in this experiment, and for low neutron energies (below 1 Mev) the detector efficiency decreases with decreasing neutron energy. The energies of the neutrons feeding the 3.62 Mev state for an incident alpha energy of 5.50 Mev are given in table 2.1.

(b) Method of Analysis

The experimental results were analyzed with the aid of a SDS-920 computer. A non-linear gaussian program has been used which fits the photo-peak with a gaussian distribution and subtracts the background from the photo-peak with constant, linear, quadratic or exponential functions. The parameters used to describe the peak are the standard deviation and the mean.

For the angular distribution results, the best fit was obtained with a quadratic background function.

The analysis of the n-γ correlation results became difficult for a gamma detector position of 0°. Results were also obtained at angles of 45° and 90° and indicated a strong correlation for the 1.59 Mev gamma ray, with the intensity minimum occurring at 0°. A strong correlation would enable a clear cut decision to be made with regard to the spin of the 3.62 Mev state, however the computer recognized a peak at 0° for only 5 of the 13 runs taken.

In order to be able to compare the other 8 runs at 0° with the corresponding runs at 45° and 90°, an analysis was carried out using line shape techniques. This type of analysis is necessary for complex spectra since the background underneath the photo-peak to be analyzed may contain the Compton edge from another photo-peak. For example, if two peaks P_1 and P_2 are separated by 300 kev. then P_1 will be located on the Compton edge of P_2. If P_2 is a strong correlation, the intensity of it's Compton edge will vary rapidly with angle, hence the background underneath P_1 is constantly changing with angle. By using a line shape for P_2, the height of the Compton edge is known and can be subtracted from P_1.

Figure 3.8 illustrates a typical n-γ coincidence for which the photo-peak due to the 1.59 Mev radiation is to be analyzed. The location of the Compton rise of the 2.43 Mev photo-peak is given by;

$$E_c(2.43) = 2.43 - \frac{2.43}{1+\frac{2\times 2.43}{m_o c^2}} \approx 2.20 \text{ Mev}$$

The Compton edge of the 2.43 Mev photo-peak is given by A in figure 3.8.

A line shape for the 2.03 Mev photo-peak was obtained from a Sb^{124} spectrum which includes a gamma ray of 2.09 Mev. The peak to Compton ratio for the 2.09 Mev radiation was found to be 1.6, the gamma spectrum being recorded by the 3"×3" detector used in the experiment. The height of the 2.03 Compton edge is given by B in figure 3.8. The area of the 1.59 Mev photo-peak above B is then used as a measure of the intensity of the 1.59 Mev radiation at that angle. No correction was made for the Compton edge of the 1.79 Mev gamma ray since it's photo-peak intensity was observed to be essentially constant with respect to the angular position of the gamma detector.

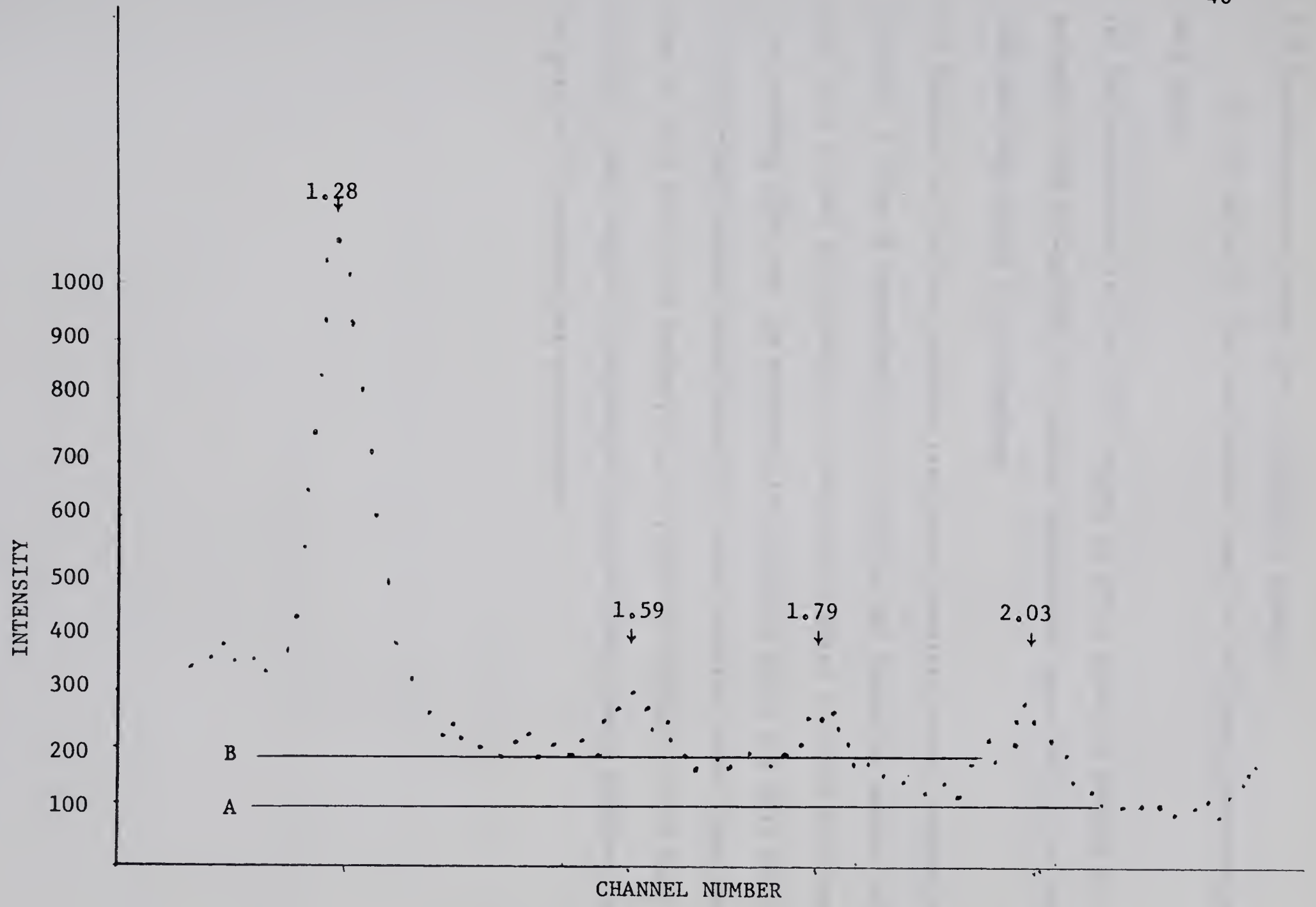

Fig. 3.8 Line Shape Analysis of n-γ Coincidence Spectrum

3.2 Considerations based upon Preliminary Results

On the basis of the preliminary runs the following observations were made;

(a) The photo-tube for the 3"×3" began to drift when the number of counts exceeded 2500 per-second. To prevent appreciable gain drift, the beam current was kept below 0.15 u-amperes.

(b) Because of the low counting rate which resulted from a reduced beam current, a time of approximately 45 minutes was needed to gather sufficient data (over 200 counts) for the neutron gated 1.59 Mev photo-peak. This running time was the maximum time possible since the gain shift of the photo-tube became significant for longer running times. Data was gathered at only the three angles; 0°, 45°, and 90° because of the time restrictions. Each angular distribution run took less than 5 minutes, hence no gain shift problem was encountered.

CHAPTER IV

Experimental Results

4.1 Angular Distribution

The measured angular distributions of the 1.28 Mev and 2.03 Mev gamma rays are shown in figures 4.1 and 4.2, respectively. The results from previous work (Br 57) are also given for comparison purposes. The measured distributions for both radiations are in good agreement, especially for the isotropic type pattern of the 1.28 Mev distribution.

The measured distribution of the 1.59 Mev gamma ray is shown in figure 4.3. The predicted angular distribution functions for the two possible spin assignments, $^5/_2$ or $^7/_2$ to the 3.62 Mev state are:

$$(1)\quad {}^{5}/_{2}\quad W(\theta)=1+\left[\frac{P(\tfrac{1}{2})\left\{.46+1.08\delta-.2\delta^2\right\}+P(\tfrac{3}{2})\left\{.11+.27\delta-.05\delta^2\right\}+P(\tfrac{5}{2})\left\{-.57-1.35\delta+.26\delta^2\right\}}{1+\delta^2}\right]\times Q_2P_2\cos\theta$$

$$+\frac{.37P(\tfrac{1}{2})\delta^2+.55P(\tfrac{3}{2})\delta^2-.18P(\tfrac{5}{2})\delta^2}{1+\delta^2}Q_4P_4\cos\theta$$

$$(2)\quad {}^{7}/_{2}\quad W(\theta)=1+\left[\frac{P(\tfrac{1}{2})\left\{-.33+2.1\delta+.08\delta^2\right\}+P(\tfrac{3}{2})\left\{-.19+1.2\delta+.05\delta^2\right\}+P(\tfrac{5}{2})\left\{+.06-.41\delta-.02\delta^2\right\}}{1+\delta^2}\right.$$

$$\left.+\frac{P(\tfrac{7}{2})\left\{.45-2.9\delta-.12\delta^2\right\}}{1+\delta^2}\right]Q_2P_2\cos\theta+\frac{\delta^2\left\{.65P(\tfrac{5}{2})+.21P(\tfrac{7}{2})\right\}}{1+\delta^2}Q_4P_4$$

In order to be able to compare the predicted distributions with the experimental distribution, assumptions concerning the population parameters appearing in equations (1) and (2) must be made. Litherland has previously determined the population parameters for the 2.03 Mev and 2.43 Mev states (Li 60), and his results are given in Table 4.1.

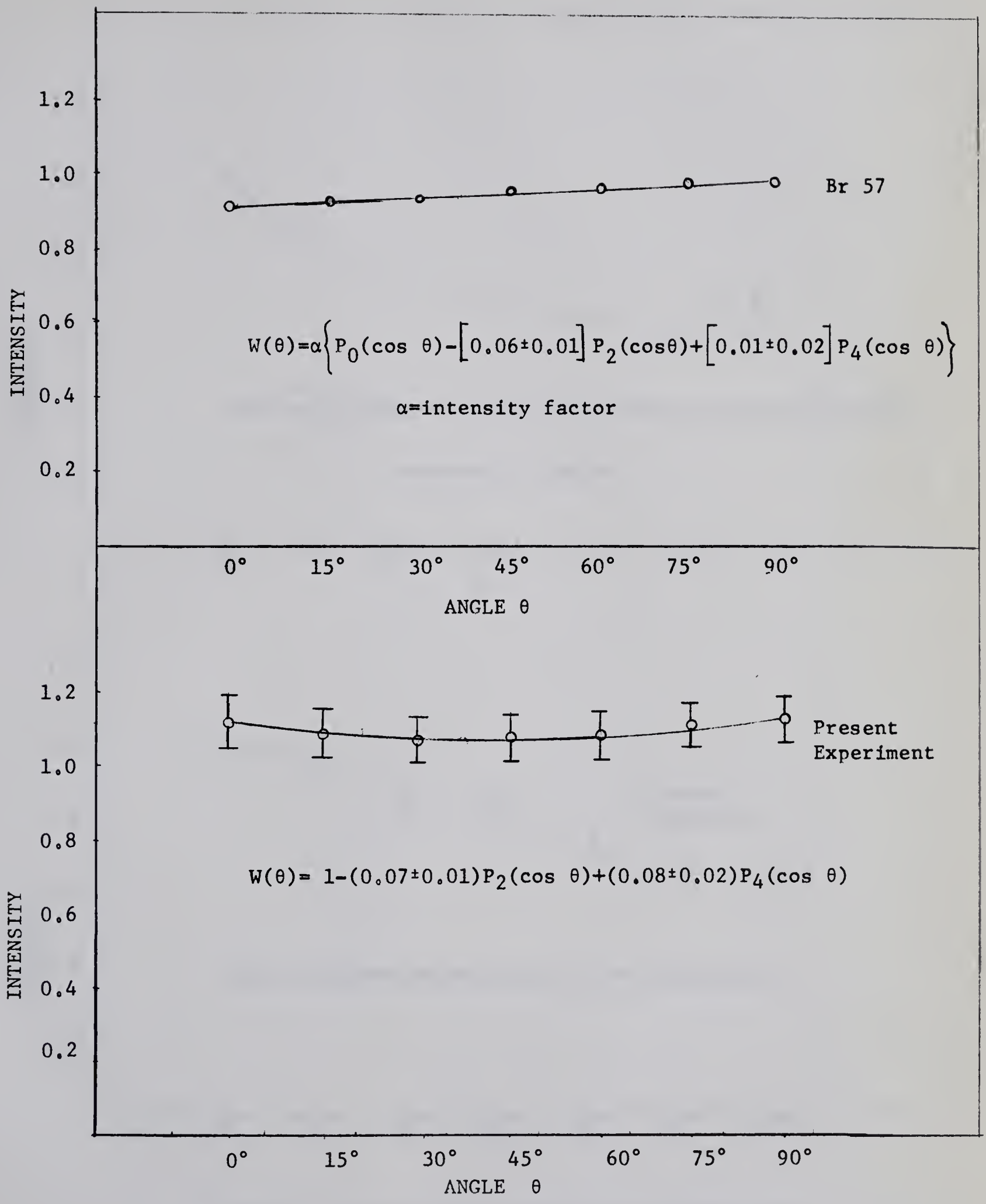

Fig. 4.1 Angular Distribution of 1.28 Mev Gamma

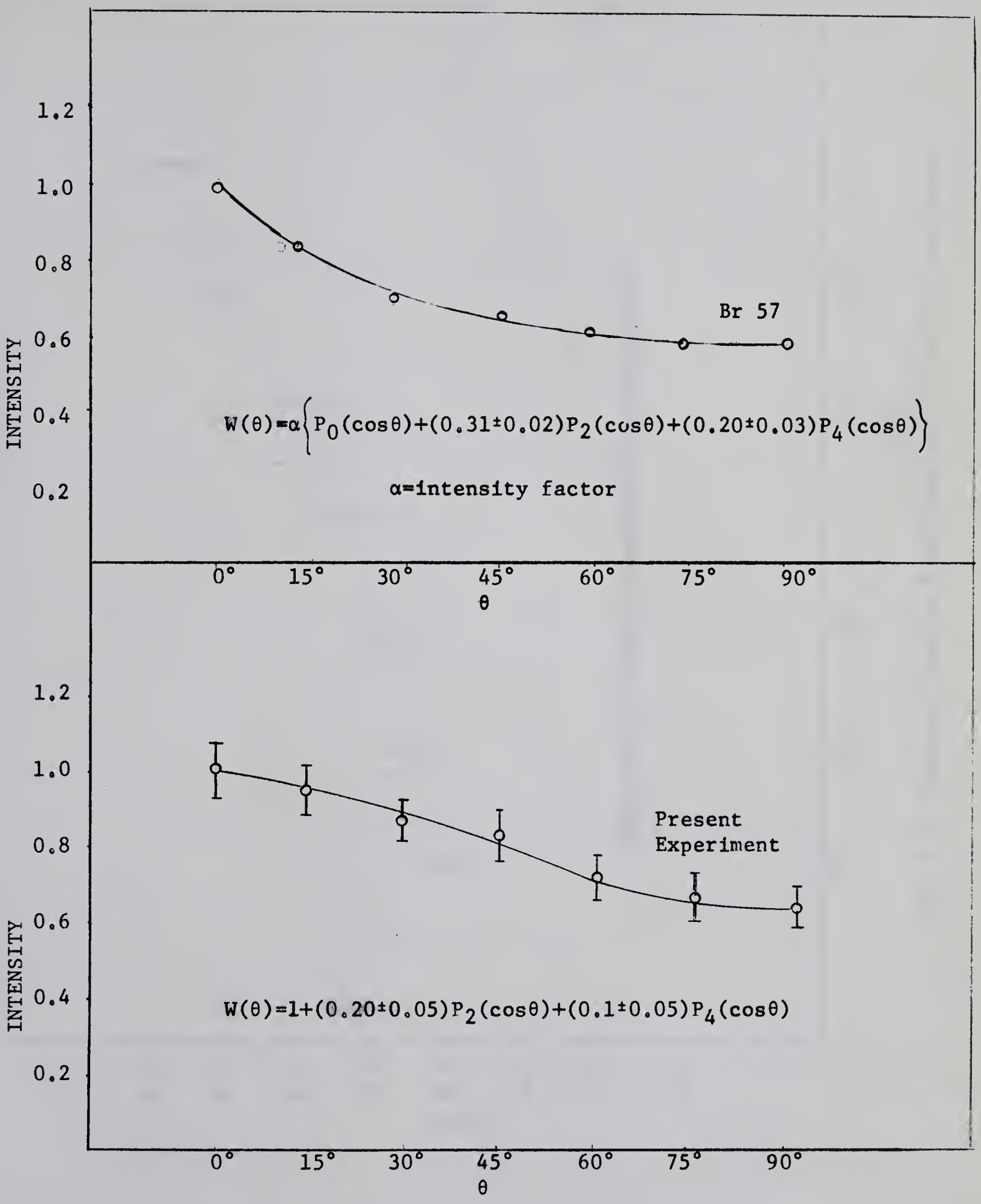

Fig. 4.2 Angular Distribution of 2.03 Mev Gamma

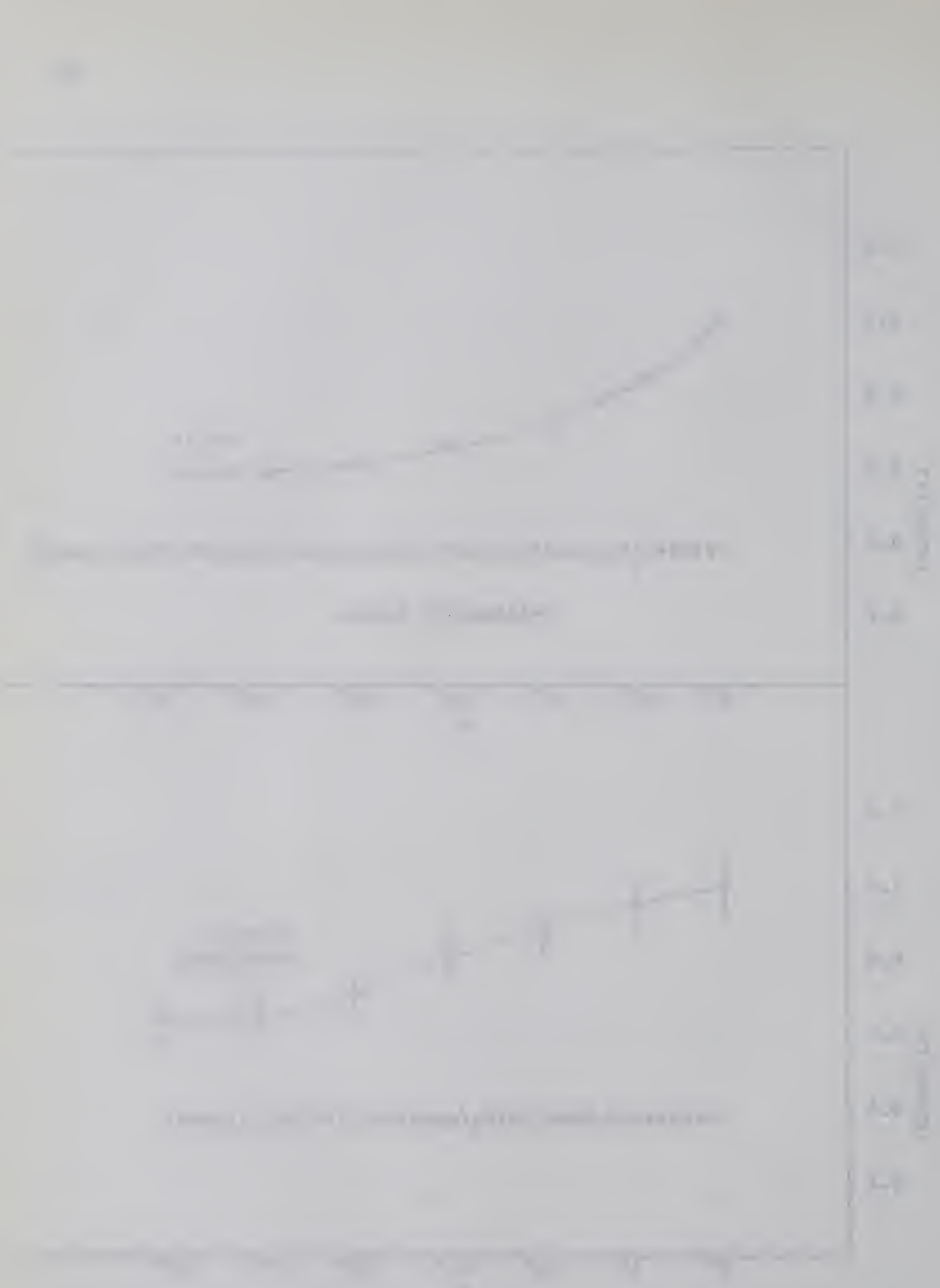

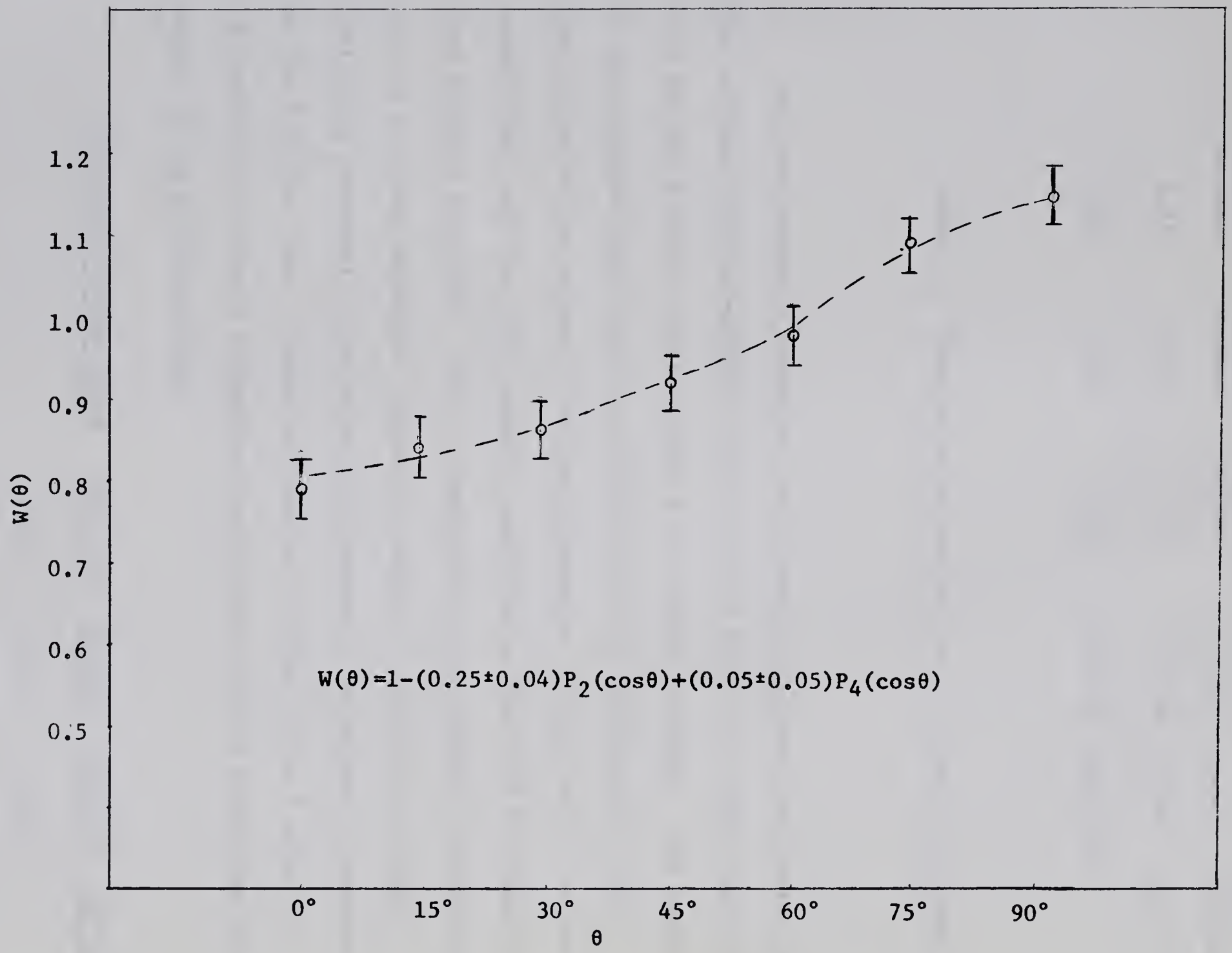

Fig. 4.3 Measured Angular Distribution of the 1.59 Mev Gamma

E_α(Mev)	E_γ(Mev)	E_n(Mev)	$P(\pm 1/2)$	$P(\pm 3/2)$	$P(\pm 5/2)$
4.74	2.03	2.49	0.36±.04	0.12±04	0.02±.03
4.94	2.43	2.49	0.41±.04	0.09±.04	

Table 4.1 Population Parameters for 2.03 and 2.43 states

The lower magnetic substates are strongly populated, indicating that the neutrons with the energies given by En in Table 4.1, which feed the 2.03 Mev and 2.43 Mev levels, carry a low angular momentum. The energy of the neutrons which feed the 3.62 Mev state is substantially lower than either of the values of En (See Kinematics 2.2(a)), and it is reasonable that only the lower magnetic substates of the 3.62 Mev state become strongly populated. This is supported by the measured distribution for the 1.59 Mev radiation, figure 4.3, which is found to be strong, indicating substantial population differences in the magnetic substates of the 3.62 Mev state. Using the results of Table 4.1 as a guide, it is possible to choose a reasonable distribution for the population parameters of the 3.62 Mev state.

Spin of 3.62 Mev state	$P(\pm 1/2)$	$P(\pm 3/2)$	$P(\pm 5/2)$	$P(\pm 7/2)$
$5/2$	0.36	0.12	0.02	
$7/2$	0.35	0.11	0.03	0.01

Table 4.2 Choice of Population Parameters for 3.62 State

Figures 4.4 to 4.6 show the predicted angular distribution, based on the population parameters of Table 4.2, for mixing ratios of $|\delta|=0$, 0.1, and 0.2.

Conclusions

In the event of a $^5/_2^- \rightarrow {}^5/_2^+$ transition from the 3.62 Mev state to the 2.03 Mev state, none of the predicted angular distributions are reconcilable with the measured distribution. For $|\delta|<0.4$, the predicted distribution indicated an intensity maximum for a gamma detector position of 0°. This is in contradiction with the experimental angular distribution which indicates an intensity at 90° which is almost twice the intensity at 0° (Figure 4.3). A value of $|\delta|>0.1$ would be incompatible with an E1-M2 mixing ratio, in the absence of selection rules, which could inhibit the E1 component of radiation.

For a $^7/_2 \rightarrow {}^5/_2$ transition, the best theoretical fit with experiment is obtained for $\delta\approx 0$, which is the most probable value for an E1–M2 mixing ratio. As δ increases negatively, the predicted distribution becomes somewhat stronger than that observed by experiment. For increasingly positive δ, the predicted distribution assumes an isotropic pattern for $\delta\approx 0.15$.

Thus the angular distribution results strongly favor a spin assignment of $^7/_2$ to the 3.62 Mev state and a mixing ratio close to zero for the resultant 1.59 Mev gamma radiation. Since assumptions were made with regard to the population parameters of the 3.62 Mev state, the result is not entirely conclusive. To help remove any ambiguities, the results of an angular correlation experiment are presented.

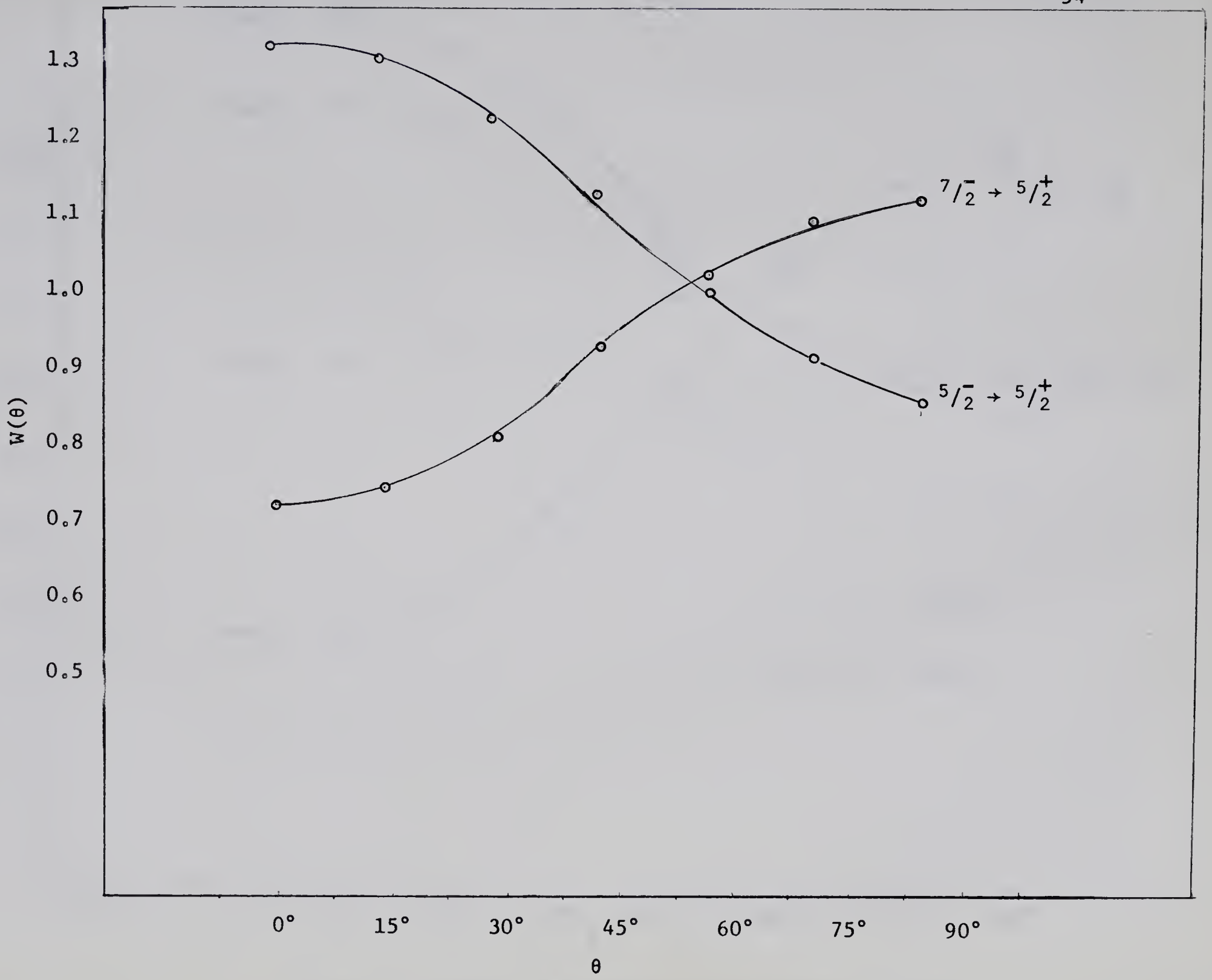

Fig. 4.4 Predicted Angular Distributions for $\delta=0$

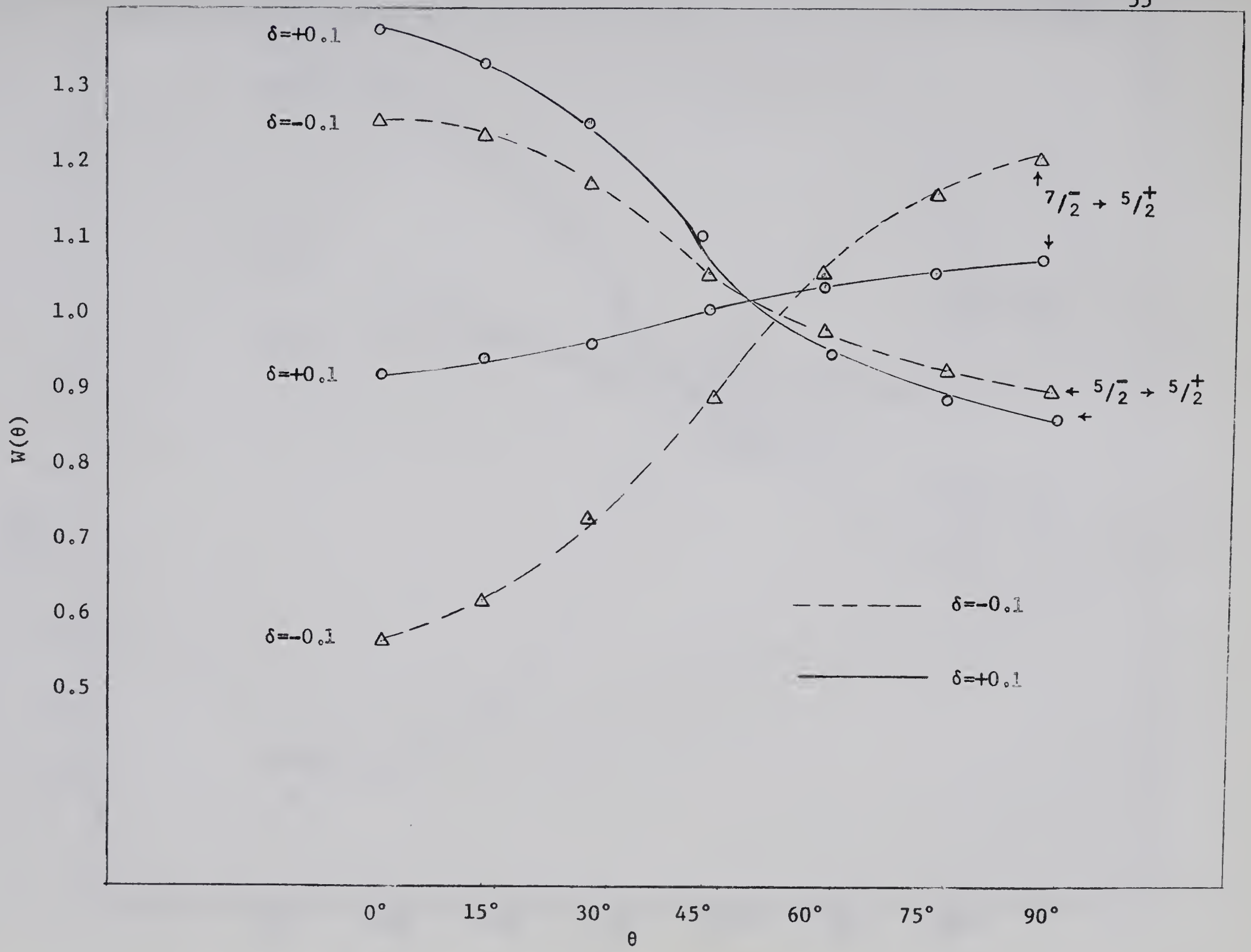

Fig. 4.5 Predicted Angular Distribution for $|\delta|=0.1$

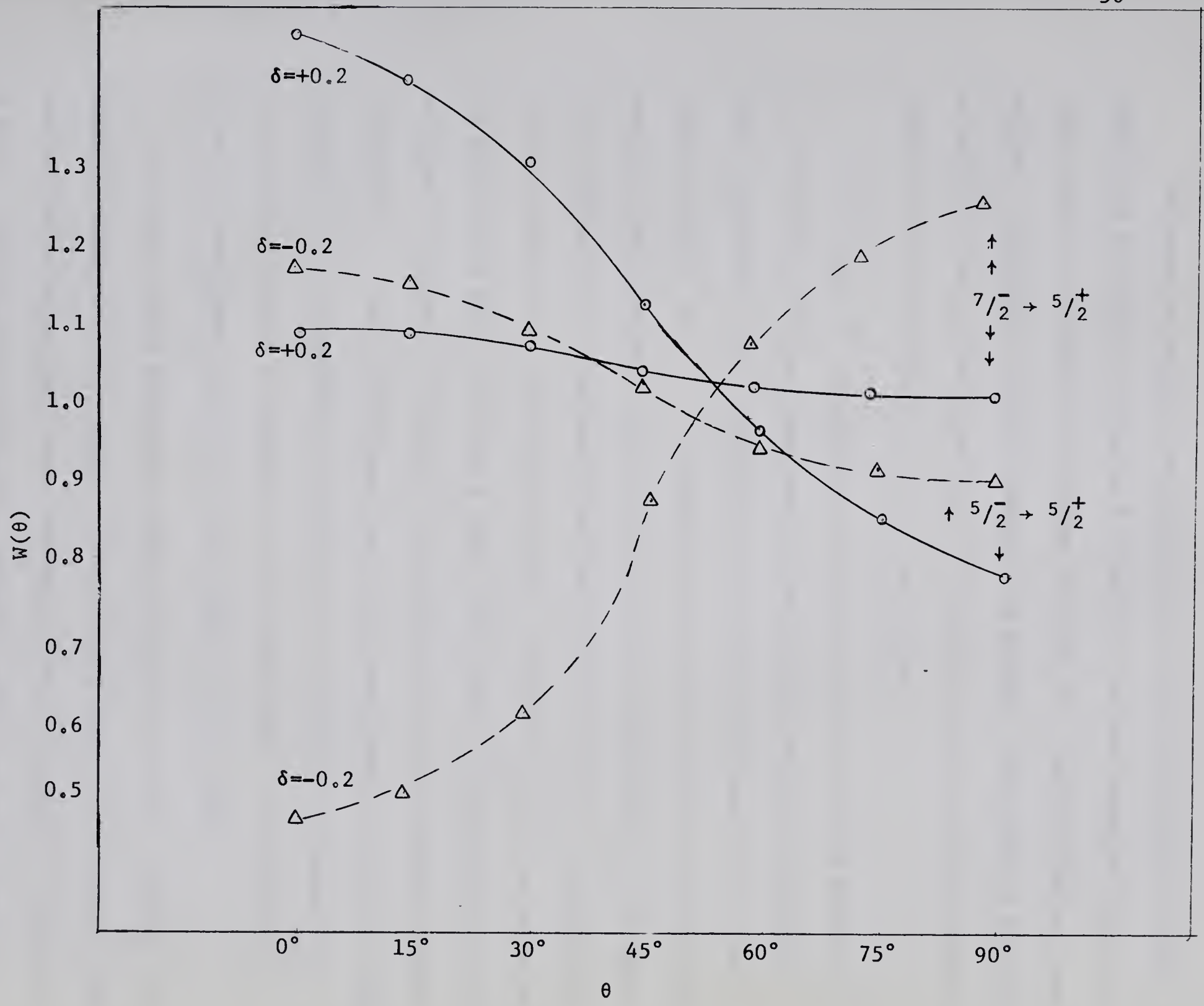

Fig. 4.6 Predicted Angular Distribution for $|\delta|=0.2$

4.2 Angular Correlation

The measured angular correlations for the 2.03 Mev and 2.43 Mev radiations are given in figures 4.7 and 4.8, and are compared with previous results obtained by Litherland (Li 60). The results from both experiments essentially overlap, however the present experiment is not able to ascertain an a_4 coefficient for the 2.03 Mev correlation since experimental data was obtained at only three angles.

The results of 5 angular correlation runs at the three angles; 0°, 45°, and 90°, which were analyzed by the SDS-920 computer, and eight other correlation runs, analyzed by line shape techniques (3.2 b) are presented in 'a' and 'b' of figure 4.9. The error bars for the line shape analysis have been made equal to the error bars determined by the computer. Because the two methods of analysis yield similar a_2 coefficients, the five computer analyzed runs were also analyzed by the line shape method and grouped with the other 8 runs. The results of the grouped 13 runs are given in figure 4.10 and will be referred to as the measured angular correlation of the 1.59 Mev gamma ray. With experimental results at only 3 angles, it is impossible to evaluate an a_4 coefficient, however for the predicted angular correlation, the a_4 coefficient is multiplied by δ^2 and the resultant term will be very small if δ is small.

For pure s-wave neutrons feeding the 3.62 Mev level, only the $m=\pm 1/2$ magnetic substates are populated. However since the neutron detector subtends a finite angle, and p-wave neutrons, from a possible 2^+ resonance in Si^{30}, could feed this state, the magnetic substates $m=\pm 3/2$ may be

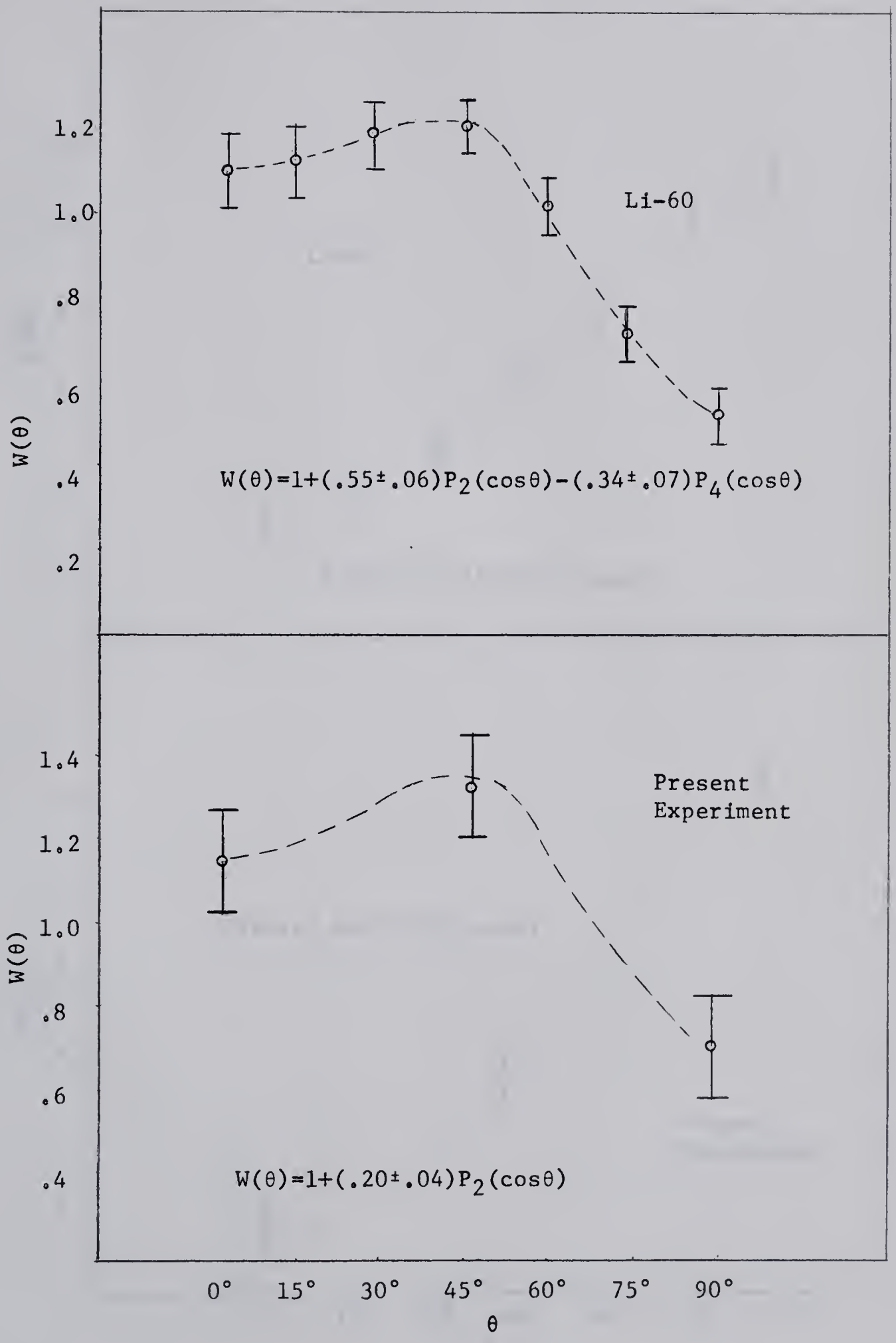

Fig. 4.7 Angular Correlation of 2.03 Gamma

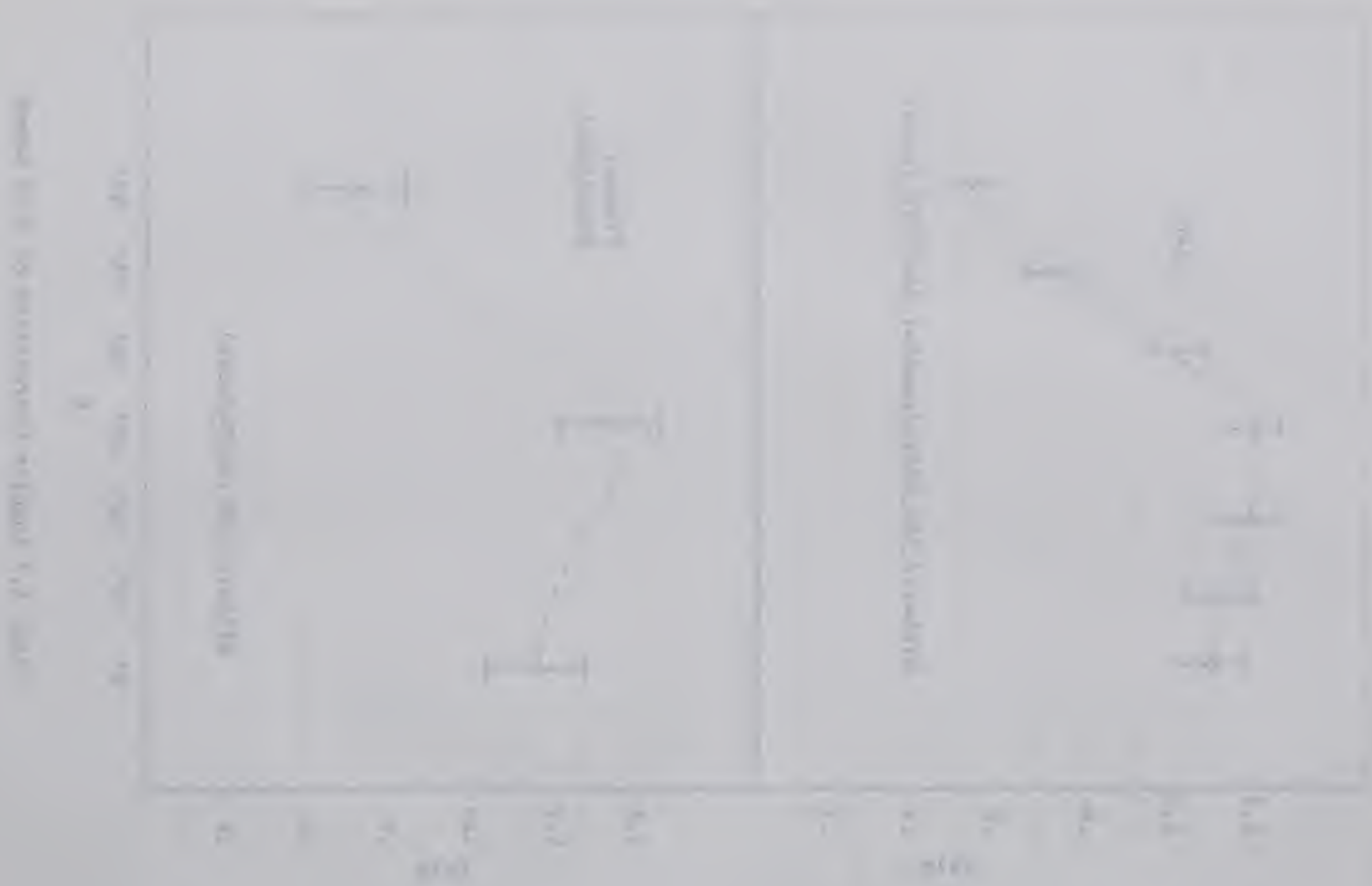

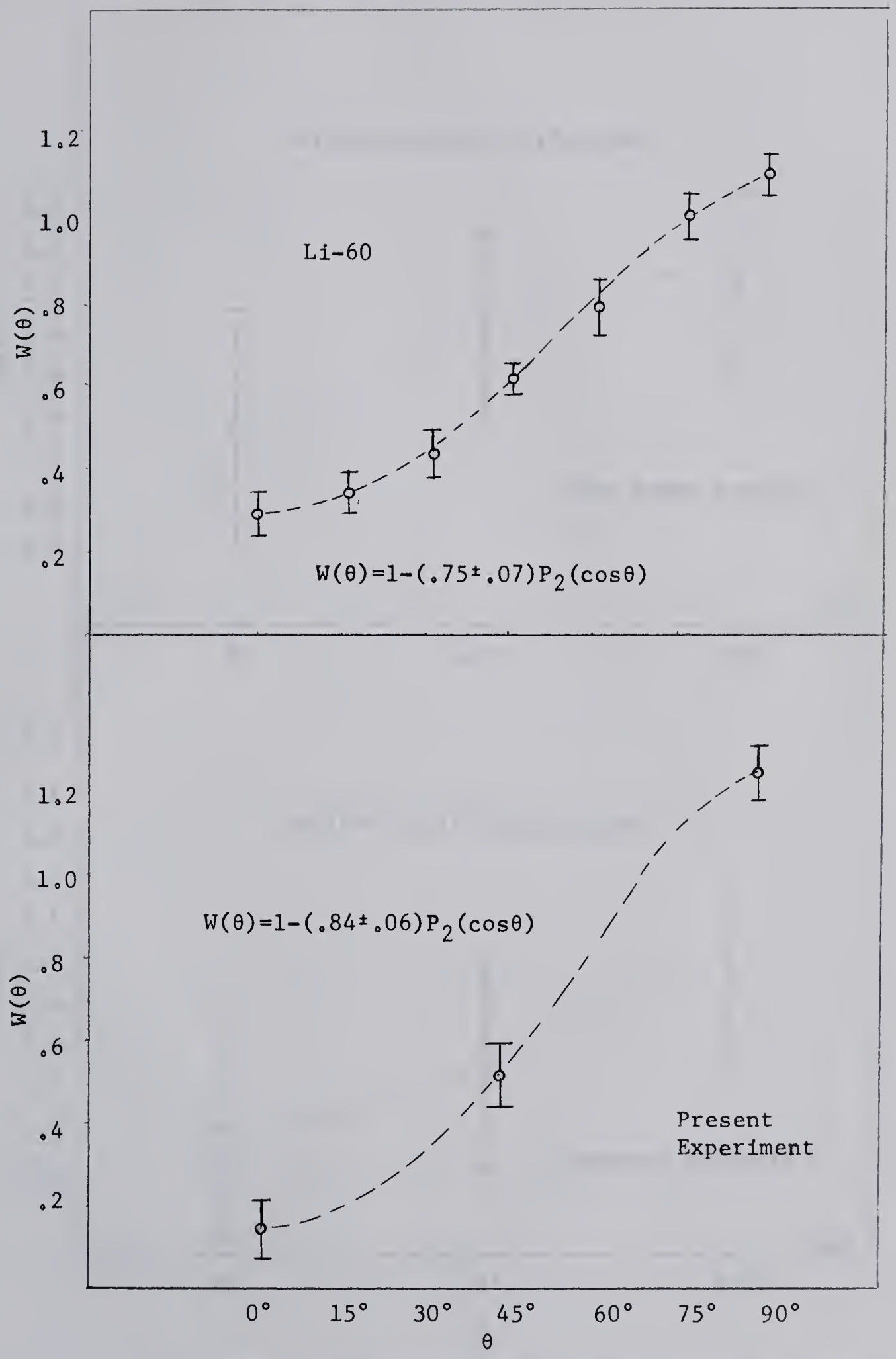

Fig. 4.8 Angular Correlation of 2.43 Gamma

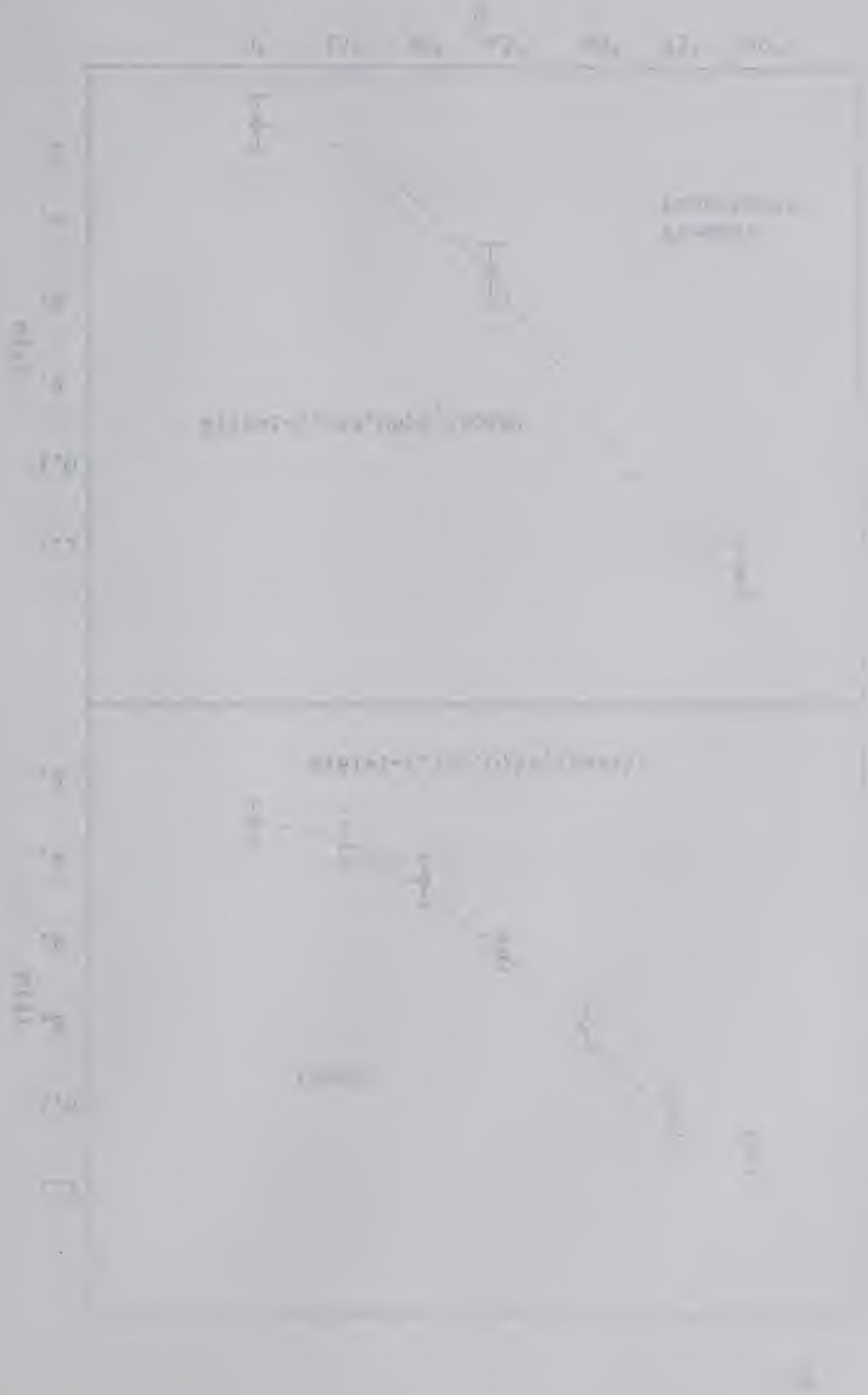

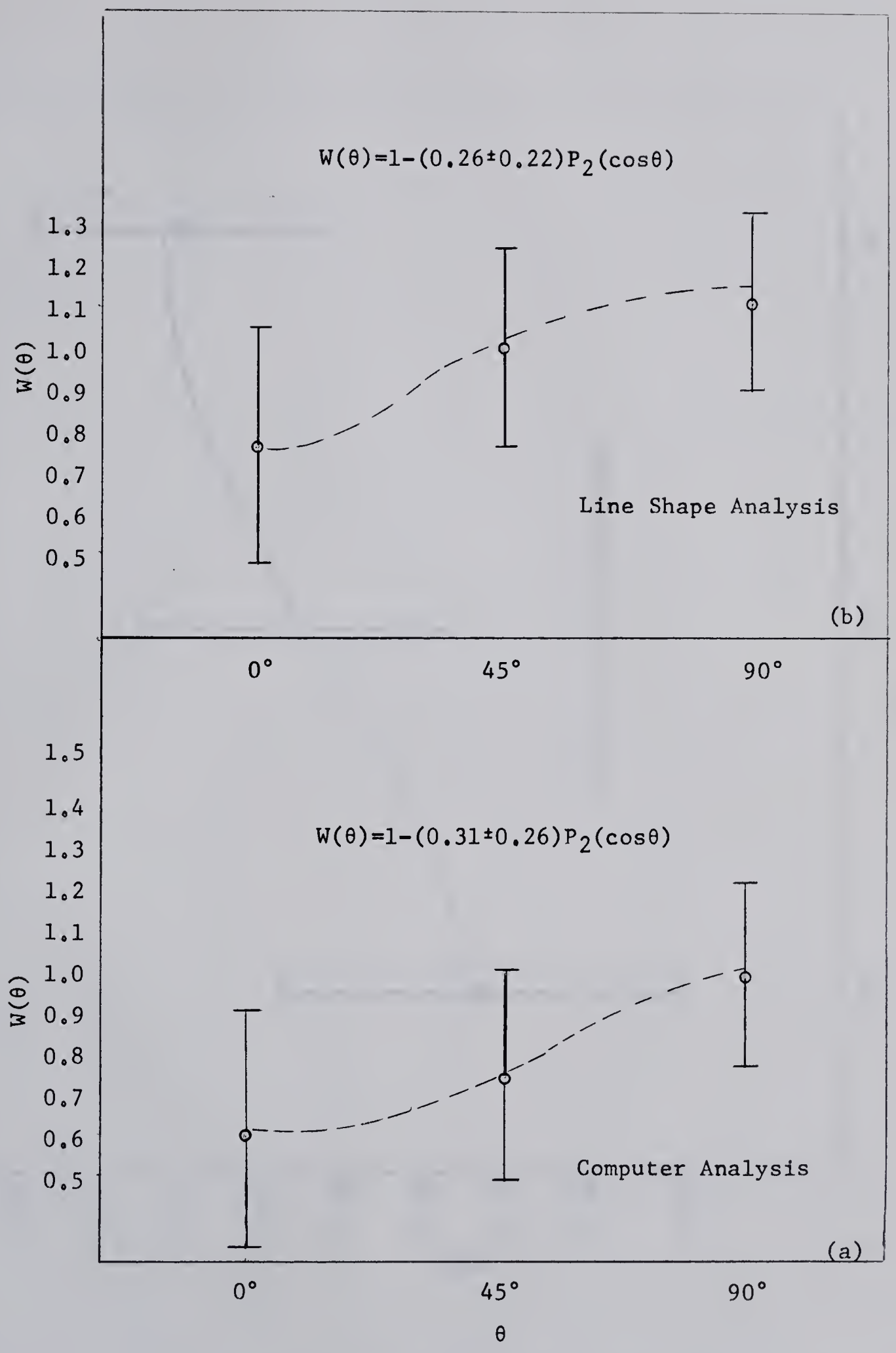

Fig. 4.9 Measured Angular Correlation for 1.59 Gamma

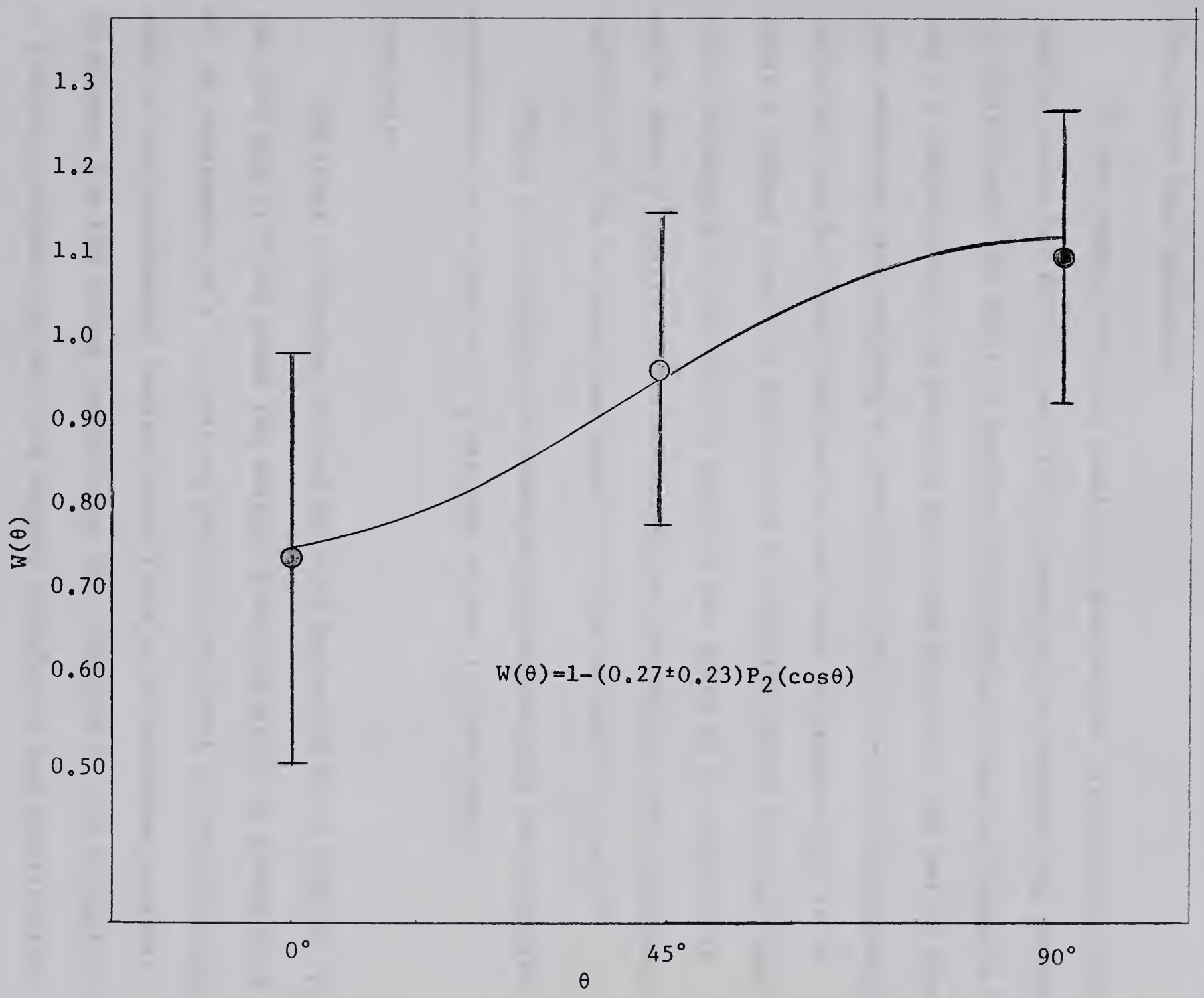

Fig. 4.10 Measured Angular Correlation of 1.59 Gamma

populated. Because of the low neutron energies involved, admixtures such as d-wave neutrons to s-wave neutrons or f-wave neutrons to p-wave neutrons, have been neglected.

If one assumes $\delta=0$, the results of the angular distribution can be used to solve for $P(\pm 1/2)$ and $P(\pm 3/2)$. Equating the measured and predicted a_2 coefficients for the 1.59 angular distribution, given in figures 4.3 and 4.4 respectively, and assuming that only the $m=\pm 1/2$ and $m=\pm 3/2$ magnetic substates are populated so that $P(\pm 1/2)+P(\pm 3/2)=0.5$, the population parameters can be found. The results are given in figure 4.11. It is readily evident from this figure that no solution exists for the population parameters if the spin of the 3.62 Mev state is $5/2$ since this would imply a negative value for one of the parameters. The simultaneous solution of the two equations gives $P(\pm 1/2)=0.32$ and $P(\pm 3/2)=0.18$

Figure 4.12 compares the measured correlation with the predicted correlation for a spin of $7/2$ assigned to the 3.62 Mev state.

Conclusion

The final conclusion is that the 3.62 Mev state has a spin of $7/2$ and that the 1.59 Mev gamma ray emitted from this state is almost pure E1. An assignment of a $5/2$ spin to the 3.62 Mev level is completely negated by the experimental results since there is no mechanism possible to account for the strong intensity at 90°, compared to the intensity at 0°, which is evident in both the angular correlation and distribution. Even allowing for substantial population of the higher magnetic substates and extreme values for the mixing ratio ($|\delta|<0.4$), the predicted

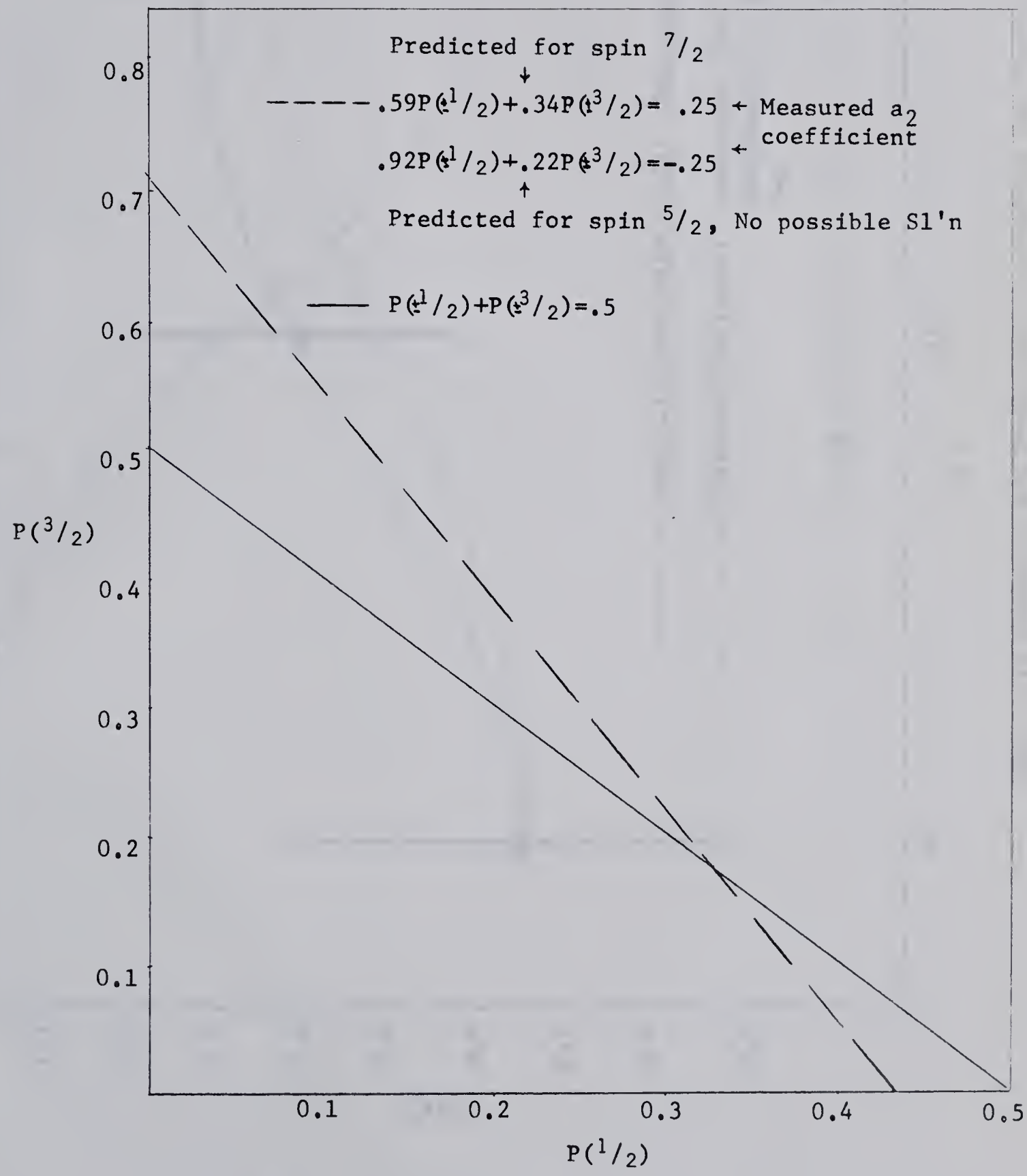

Fig. 4.11 Solution for the Population Parameters;δ=0

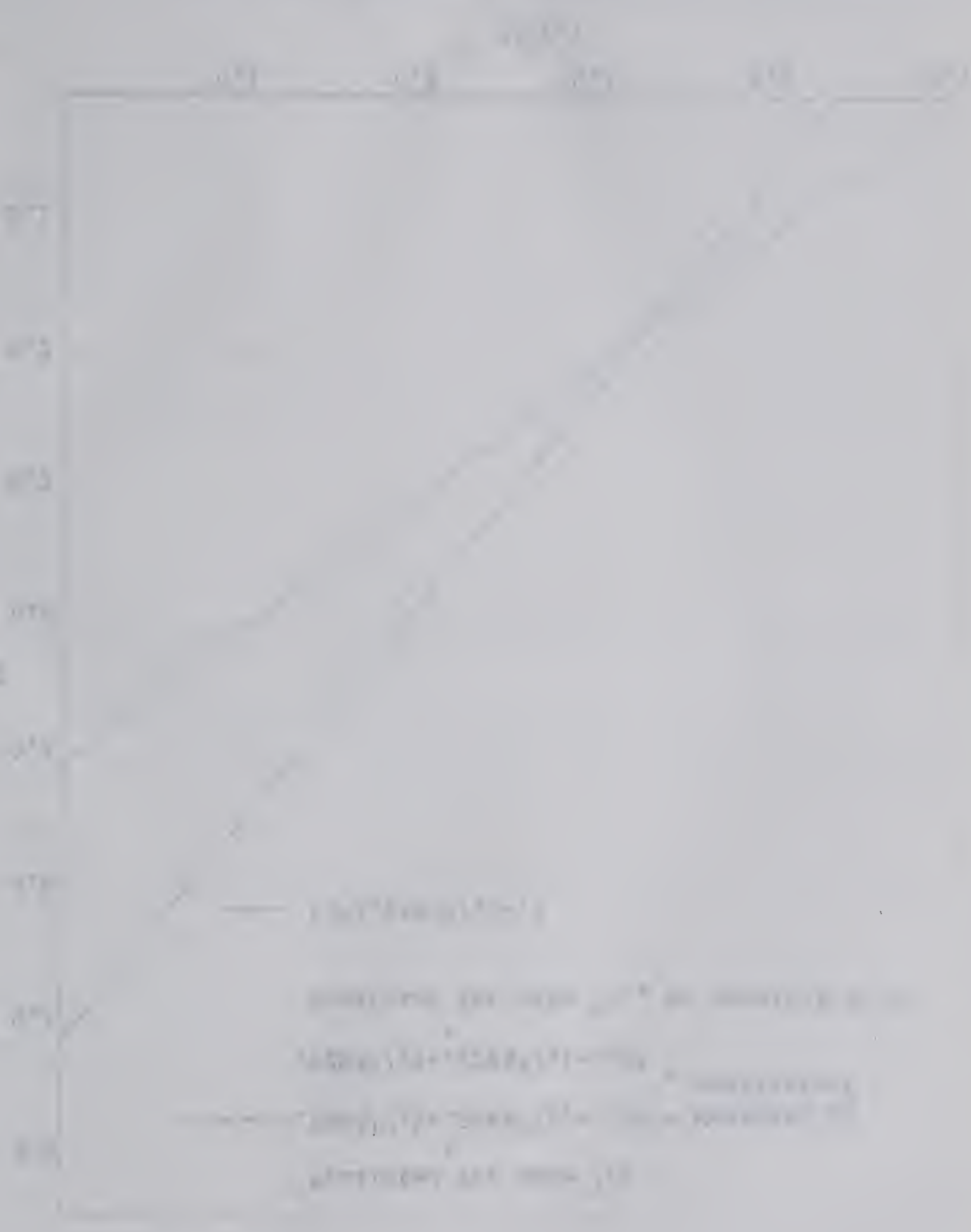

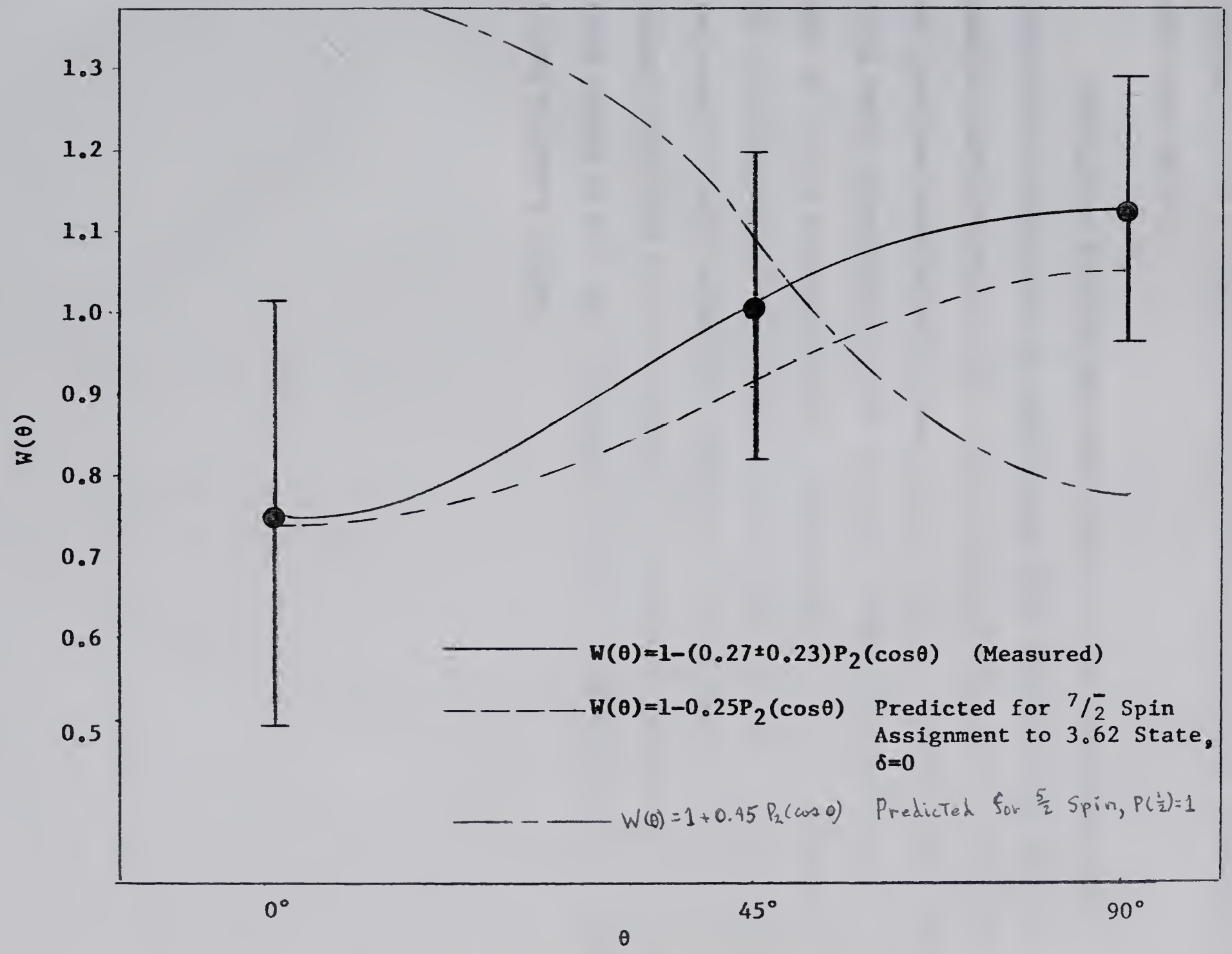

Fig. 4.12 Measured and Predicted Correlation for the 1.59 Gamma

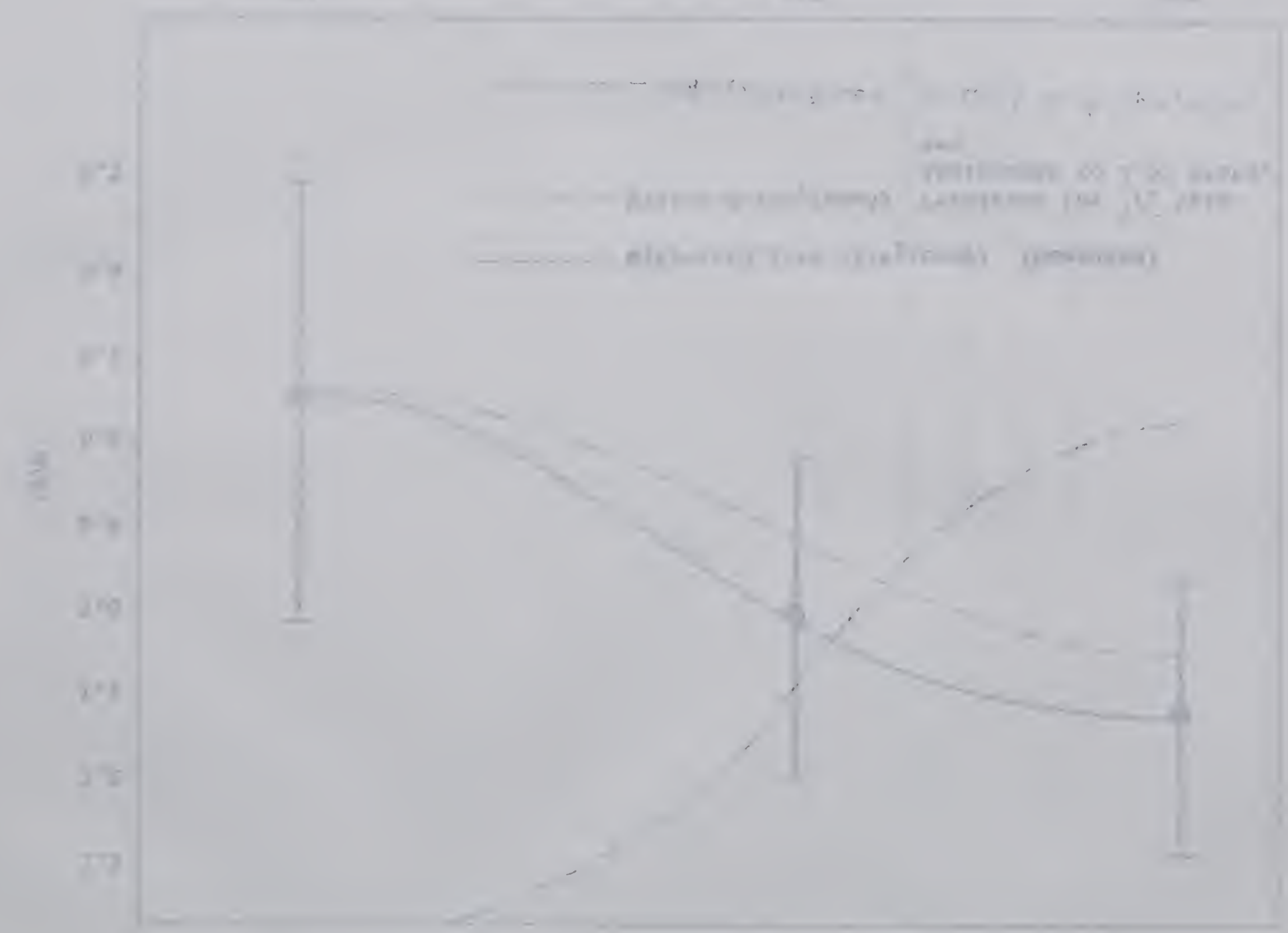

correlation for a $^{5}/_{2}^{-} \rightarrow {}^{5}/_{2}^{+}$ transition indicated the maximum intensity should occur at 0°.

Although no analysis was done on the 1.79 Mev radiation emitted from the 3.07 Mev state, the experimental data indicated that the 1.79 angular distribution was weak. From stripping curves (Ho 53), the 3.07 Mev level was ascertained to have a spin of $^{3}/_{2}$ or $^{5}/_{2}$ and recent branching ratio measurements (Se 59) have led to the conclusion that the spin is $^{5}/_{2}$. If the spin of the 3.07 Mev state is $^{5}/_{2}$, an explanation for the occurrence of an isotropic distribution for the 1.79 Mev radiation would be that a substantial admixture of E2 radiation occurs in the mixing ratio. This is in accord with the rotational character of the low-lying states in Si^{29} and is mentioned further in the discussion of results in the following chapter.

CHAPTER V

Rotational Model Aspects of Si^{29}

A spin assignment of $^{7}/_{2}$ to the 3.62 Mev level indicates that the Si^{29} nucleus possesses a negative spheroidicity. ie., oblate shape (see 1.2) It has been previously been determined that the nucleus Al^{28} has a positive spheroidicity which corresponds to a prolate shape (Sh 56). Thus the equilibrium deformation of d-s shell nuclei changes sign in the mass region at A=28.

For an oblate shape, the sequences of rotational levels in Si^{29} are based on the $K=^{1}/_{2}$ ground state and the $K=^{3}/_{2}$ state at 1.28 Mev. The members of the $K=^{1}/_{2}$ band are the levels at 2.03 Mev and 2.43 Mev; the 3.07 Mev state is built on the $K=^{3}/_{2}$ band. Another possible rotational sequence could originate from a $K=^{1}/_{2}$ band based on Nilsson orbit 11 (1.2), however no experimental evidence for the existence of this higher lying sequence, above 4.5 Mev, has yet been found. The 3.62 Mev state, which has been considered extensively in the present experiment, is a good single particle $1f^{7}/_{2}$ state (1.2). The next odd parity level in Si^{29} which has been observed, occurs at 4.89 Mev and has been assigned a spin of $^{3}/_{2}$ (Ma 59). Theoretical arguments (Ch 63) have been given for a spin assignment of $^{7}/_{2}$ and positive parity to the 4.08 Mev state which would indicate it to be a member of either the $K=^{1}/_{2}$ or $K=^{3}/_{2}$ bands.

The 1.79 Mev transition occurs between the 3.07 Mev and 1.28 Mev levels which are members of the same band. The weak distribution observed for this radiation, mentioned in 4.2, indicates a substantial mixing ratio which would be in accord with the rotational sequence given above.

The M1-E2 mixing is large because E2 enhancement occurs between members of the same band (Br 57).

It is interesting to consider two other decay modes for the 3.07 Mev state; those of gamma transitions to the levels at 2.03 Mev and ground state. A mixing of M1-E2 radiation occurs for the 1.04 Mev transition and E2-M3 mixing for the 3.07 Mev ground state transition. In this experiment and also in Br-57, it was noted that the 3.07 state decayed via the 2.03 state approximately $^1/_4$ of the time, whereas no evidence for the 3.07 transition was found. This would indicate that the 1.04 Mev radiation is predominantly M1 in nature.

The predictions of the Nilsson generalized single particle model with regard to Si^{29} have been found to be strongly substantiated by experimental data gathered on the low-lying states. In this model, the single particle moves in the field of a permanently deformed core of Si^{28}, which has been found to possess an oblate shape in the present experiment. It would be expected that as one applies this model to the higher levels of Si^{29}, the agreement with experiment would become less striking since the rotational core-particle coupling becomes appreciably weaker. Further experimental data on the higher levels would be beneficial in order to perhaps measure the spatial extent of the core field and to understand the origin of these higher levels.

Many nuclei in the $1d^3/_2$-$2s^1/_2$ shell have been found to possess low-lying energy states which originate from the rotational motion of some core. Further experimental work on these nuclei in the mass region

A=31 would prove interesting, in order to find the limit of applicability of the rotational model in this mass region. The existence of such a limit would then have to be related to the configuration of the nucleons composing the nucleus and hence a further understanding of the nucleus itself would be possible.

Appendix

We have, from (6) of 1.2

$$W(\theta,c) = \sum_{m_i m_f} \sum_{\substack{MM' \\ \mu\mu'}} \sum_{kmm'} P(m_i)\ \overline{\alpha}_{LM}(c)\alpha_{LM}(c)(L-\mu L\mu'|km)(LLMM'|km') \tag{1}$$

$$\times\ D^{k}_{mm'}(0\theta 0)\overline{\langle j_f m_f|T^{\mu'}_{L}|j_i m_i\rangle\langle j_f m_f\ T^{\mu}_{L}\ j_i m_i\rangle}$$

Using Racah's notation (Ra 42), one can introduce the V coefficient which is given by

$$V(J_1 J_2 J; m_1 m_2 - m) = (-1)^{J-m}(2J+1)^{-1/2}(J_1 J_2 m_1 m_2|Jm)$$

The V coefficient is related to the matrix element of (1) by

$$\langle j_f m_f|T^{L}|j_i m_i\rangle = (-1)^{j_i - m_i}\langle j_f||T^{L}||j_i\rangle\ V(j_i j_f L; -m_i m_f \mu) \tag{2}$$

The V coefficient can also be related to a Clebsch-Gordon coefficient appearing in (1)

$$(L-\mu\ L\mu'|km) = (-1)^{k+m}\ (2k+1)^{1/2}\ V(LLk; -\mu-\mu'-m) \tag{3}$$

Putting (2) and (3) into (1) gives

$$W(\theta c) = \sum_{m_i m_f} \sum_{\substack{MM' \\ \mu\mu'}} \sum_{k,mm'} P(m_i)\overline{\alpha}_{LM}(c)\ \alpha_{LM}(c)(2k+1)^{1/2}\ D^{k}_{mm'}(0\theta 0) \tag{4}$$

$$\times\ (LLMM'|km)\ V(j_i j_f L; -m_i m_f \mu)\ V(j_i j_f L; -m_i m_f \mu')V(LLk; -\mu\mu' m)$$

The relation of the V coefficient to the Racah coefficient is given below, using Racah's notation.

$$(-1)^{f+\eta}\ V(abe;\alpha\beta-\varepsilon)V(afc;-\alpha\phi\gamma)\ V(fbd;\eta\beta-\delta) =$$

$$(-1)^{b+c-a-d+e+\varepsilon}\ W(aefd;bc)\ V(edc;-\varepsilon\delta\gamma) \qquad (5)$$

The elements of the coefficients are the angular momenta involved in the coupling and the magnetic quantum numbers.

Also a phase relation between the V's is

$$V(j_ij_ik;-m_im_i\mu) = V(j_ij_ik;-m_im_i0)\delta_{0m\mu}$$

Using (5) to write the product of three V coefficients in (4) as the product of a Racah coefficient and a V coefficient one finds

$$W(\theta c) = \sum_{mMM'}\ \sum_{mk}\ P(m_i)\bar{\alpha}_{LM}(c|\ D^{k}_{mm'}(LLMM'|km)(2k+1)^{1/2} \qquad (6)$$

$$x\ W(j_fj_iLk;Lj_i)\ V(j_ij_ik;-m_im_i0)$$

One can eliminate the V coefficient of (6) by using (3) and this yields the Clebsch-Gordon coefficient $(j_ij_im_i-m_i|k_0)$. Grouping the Clebsch-Gordon coefficient of (4) with the α's to form the radiation parameter $C_{km}(LL)$ gives (7) of 1.2.

BIBLIOGRAPHY

Bo 53 A. Bohr and S. Mottelson, Kgl. Danske Videnskab. Selskab. Mat. fys Medd. 27, No. 16, (1953)

Br 57 D. Bromley, Can. Jl. Phys. 35, 1042, (1957)

Ch 63 B. Chi and J. Davidson, Phys. Rev. 131, 366, (1963)

Cl 61 M. Clark, H. Gove, and A. Litherland, Can. Jl. Phys. 39, 1241, (1961)

Da 64 C. Davisson, Private Communication, (1964)

Da 65 W. Davies, Univ. of Alberta, to be published

Da 65' W. Davies, Univ. of Alberta, to be published

Fr 61 J. French and M. MacFarlane, Rev. of Modern Phys. 32, 664, (1961)

Go 60 E. Goulding, R. Nicholson, and J. Waugh, Nuc. Inst. and Methods, 8, 272, (1960).

Ho 53 J. Holt and T. Marsham. Proc. Phys. Soc. (London), A, 66, 467, (1953).

Li 58 A. Litherland, M. McManus, E. Paul, D. Bromley, and H. Gove, 36, 378, (1958), Can. Jl. of Phys

Li 60 A. Litherland and G. McCallum, Can. Jl. of Phys. 38, 927, (1960)

Ma 59 G. Manning and G. Bartholomew, Phys. Rev. 115, 401, (1959)

Ma 61 M. MacFarlane, and J. French, Rev. of Mod. Phys. 32, 665, (1961)

Mo 54 S. Moszkowski, Beta and Gamma ray Spectroscopy, edited by K. Siegbahn, Chap. XIII

Ni 55 S. Nilsson, Kgl. Danske Videnskab. Selskab. Mat. fys. Medd. 29, No. 16, (1955)

No 63 R. Nordhagen, Nuc. Phys. 44, 130, (1963)

Ro 53 M. Rose, Phys. Rev. 91, 610, (1953)

Se 54 B. Sears and M. Radtke, Chalk River Report TPI-75, Chalk River Ontario, (1954)

Se 59 F, Ajzenberg-Selove and T. Lauritsen, Nuc. Phys. 11, (1959)

Ya 65 M. Yates, Alpha, Beta, and Gamma ray Spectroscopy; K. Siegbahn editor, Vol. 2, Appendix 9, 1965